NYO 3510-18

ANNUAL PROGRESS REPORT

TO

THE UNITED STATES ATOMIC ENERGY COMMISSION

CONTRACT AT (30-1) 3510

BIOLOGICAL AND CLINICAL DOSIMETRY

Contract Period:	November 1, 1970 - October 31, 1971
Report Period:	July 1, 1970 - June 30, 1971
Senior Investigator:	John S. Laughlin, Ph.D., Member

Sloan-Kettering Institute for Cancer Research
410 East 68th Street, New York, N.Y. 10021

DISCLAIMER

TABLE OF CONTENTS

Table of Contents (continued)

I. SUMMARY

The fabrication of the tissue equivalent absorbed dose calorimeter for neutrons has been completed and assembly and testing are in progress.

A preliminary comparison has been made of the sensitivity of the hexahydroxyethyl pararosaniline cyanide radiochromic dosimeter to γ rays and neutrons. Results indicate that these are approximately equal and that further investigation of this system is desirable.

Measurements are continuing of the LET distributions produced by various neutron sources and a search for an optimum method of data smoothing for computer processing of this data is being pursued.

Dosimetric studies substantive to a variety of biological experiments utilizing cyclotron produced neutrons and ^{252}Cf spontaneous fission sources are in progress.

Pulsed electron sources such as 600 kV field emission generators can deliver doses in excess of 10^6 rads in single pulses having duration times of a few nanoseconds. When these sources are used to irradiate thin layers of cells, the measurement of absorbed dose is complicated by the associated high dose rates, the relatively low electron energy, and the thickness of the sample which may be only a few microns. In this laboratory the problem of measuring absorbed dose has been investigated by the use of thin disks of Pilot-B, a commercially available fast response plastic scintillator. The measurement of light pulses from the scintillator was accomplished with a nanosecond pulse integrator constructed at our laboratory. The determination of the dose delivered to a cell layer made use of an extrapolation technique in which varying thicknesses of a scintillator disk are placed at the irradiation position in the same geometry as the cellular layer. A thin foil absorbed dose calorimeter was constructed to provide a calibration for the scintillator light output. Since the dynamic range of the scintillator system is quite large, it was possible to perform absorbed dose measurements over the large range of doses used for various radiobiological experiments.

A small prototype gamma camera based upon a single (2x2)cm diode of p-type ultra-pure germanium has reached an operational stage. Two dimensional information from the camera is achieved through the use of the orthogonal strip geometry developed at Sloan-Kettering in a lithium drifted silicon diode. Preliminary data indicate a spatial resolution of within (3.5x3.5) mm for Co 57 (122 kev). Evaluation of image quality is in progress.

II. NEUTRON DOSIMETRY AND ABSORBED DOSE MICROCALORIMETRY

During the current report period, our research effort on neutron dosimetry has been divided among two areas:

1) Design and construction of a tissue equivalent absorbed dose microcalorimeter to serve as a primary standard for the calibration and study of the response of other dosimetry systems to neutron irradiation.

2) Undertaking dosimetric measurements and experimental design necessary to research on the biological response of mammalian cell cultures and small animals to fast neutrons from the Institute cyclotron and ^{252}Cf spontaneous fission sources. In this work considerable effort has been expended in the utilization of a Rossi counter for the determination of LET spectra from various sources as a function of location in an irradiated medium.

A. Design and Construction of Tissue Equivalent Absorbed Dose Calorimeter

A major objective of our current research is to construct a tissue equivalent absorbed dose microcalorimeter. This will serve as a primary standard for the evaluation of the response of various dosimetry systems to fast neutrons. It has been our further intention to achieve a sufficiently high degree of compactness and durability to permit the convenient transportation of the apparatus to sources of $-\pi$ Meson or ion beams when they are available with adequate intensity for calorimetric dosimetry. This program is analagous to our work with fast electrons and gamma rays as reported in various publications.

The design of the quasiadiabatic microcalorimeter is similar to those previously constructed at our laboratory (1, 2, 3, 4) and is described at some length in our previous progress report (5). The device incorporating both active and passive thermal shields is constructed from Shonka A-150 tissue equivalent conducting plastic.* It is located in a styrofoam insulating enclosure 16" x 16" x 24" into which additional plastic segments may be placed to vary the effective depth of measurement or, alternatively, it may be placed at various depths in a tank of tissue equivalent liquid. The enclosure, or tank, serves as the primary thermal shield which can be passively controlled in a reasonably stable ambient. A tissue equivalent plastic phantom, in which ion chambers or other dosimeters are placed, can be substituted for the calorimeter. Since the maximum dose rates routinely available from our cyclotron are from 1/4 to 1/10 those obtained from the betatron, the problems of thermal stability and reduction of electrical noise in the measuring circuitry are of considerable magnitude.

---

*Obtained from the Physical Sciences Laboratory, St. Procopius College, Lisle, Ill.

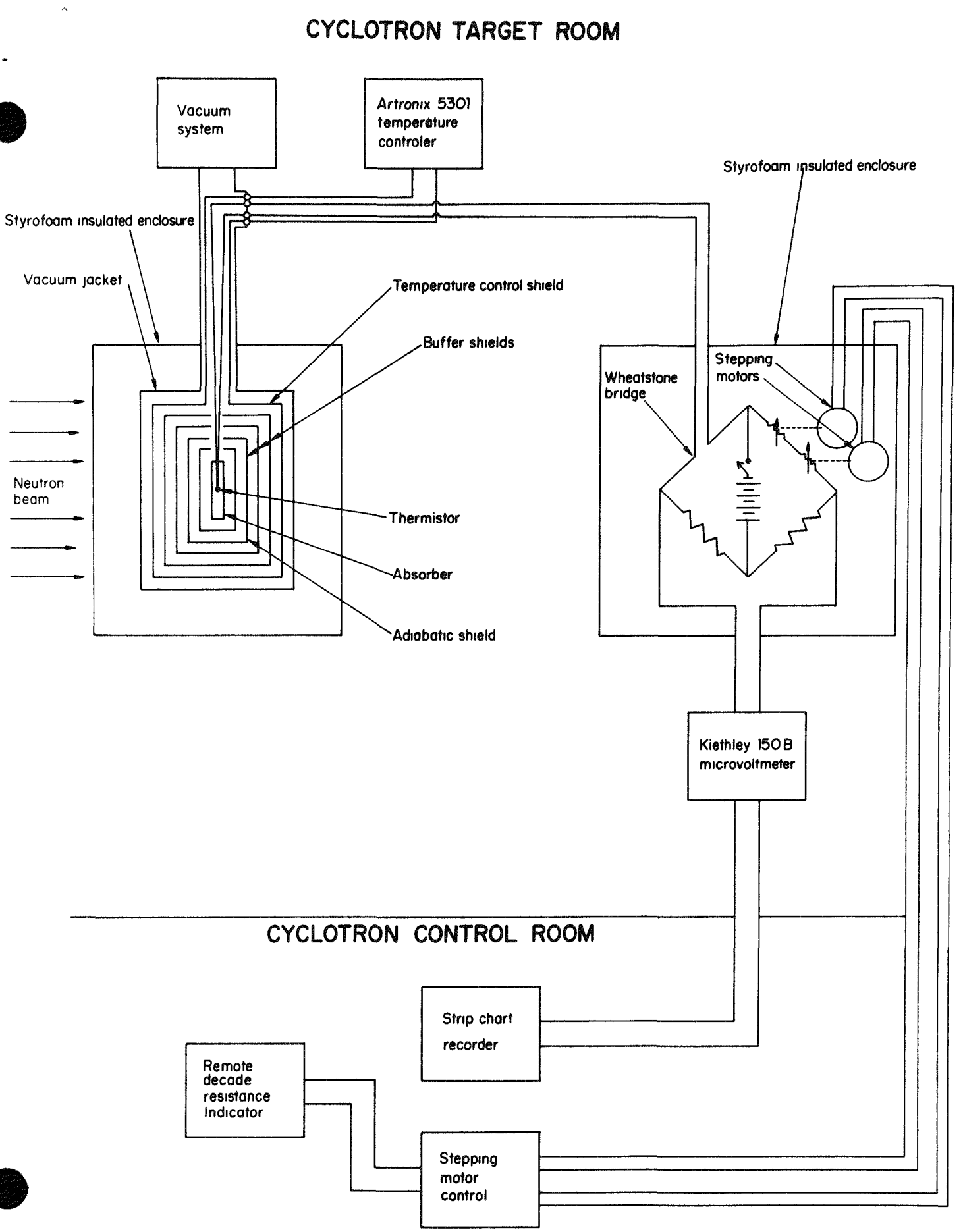

TISSUE EQUIVALENT CALORIMETER SYSTEM

Fig. I

In our design, therefore, three buffer shields are placed between the thermal control and adiabatic shields in order to improve thermal isolation. The advantages of this approach have been described by Laughlin and Genna (6). Figure I shows a schematic view of the calorimeter. The Artronix Model 5301 temperature controller** chosen for the regulation of the thermal control shield has been found capable of $\pm 0.001^{\circ}$C/hour regulation. Allowing for the expected thermal isolation, temperature fluctuations at the wafer should be of the order of 10^{-7} °C/minute and should not represent a significant source of error.

The problem of electrical noise is more difficult since an absorbed dose of 10 rads yields a signal of approximately 2 microvolts for the selected values of the thermistor and bridge resistance. Measurements of the drift and noise using an electrical mockup of the calorimeter connected to the null detector by cabling from the cyclotron target area to the control room indicated that this would prove an unsatisfactory approach. It was therefore decided to locate the null detector and bridge in close proximity to the calorimeter and to drive the resistance decade switches of the bridge by stepping motors to permit remote balancing.

In the course of our design studies it became apparent that the observed electrical resistivity of the tissue equivalent plastic is highly dependent upon the method used to make contact. For sample disks 0.5 cm thick and 3.8 cm in diameter, the resistance measured between opposing faces was approximately 150,000 ohms for large area mechanical contacts, 3000 ohms for evaporated aluminum electrodes and 20 ohms when evaporated gold contacts were applied. Moreover, with the exception of samples bearing evaporated gold electrodes, appreciable variations in resistance were observed with time.

These results posed several clear problems:

While the resistance values observed with the gold coatings were stable, they were too low to be acceptable for satisfactory electrical heating of the wafer and adiabatic shield. This is because of the large power dissipation in the relatively high resistance leads attached to these elements to assure thermal isolation. The resistances observed with aluminum electrodes are adequately high, but tend to be variable and furthermore, seem clearly indicative of a high interface resistance between the aluminum film and the body of the plastic.

In view of the above, separate metalizing and heating techniques have been chosen for the various elements of the calorimeter. The thermal control shield parts have gold electrodes applied to opposing faces providing a low, uniform load resistance for the temperature controller power supply. The adiabatic shield components and wafer, however, have aluminized elec-

---

** Obtained from Artronix Instrumentation, St. Louis, Missouri

trodes applied to opposing faces and are heated by repetitive discharges of a small capacitor. This method renders the power dissipated in the load independent of load resistance. Because of the relatively small thickness of these components, the generation of heat at their surfaces should provide a satisfactory simulation of the heating produced by the radiation field. The calorimeter is currently undergoing final assembly and testing and actual measurements utilizing it will be begun within the current contract period.

B. Response of Secondary Dosimeters to Neutron Irradiation

McLaughlin and others (7, 8, 9) have reported on the development of high sensitivity radiochromic dosimeters for fast electrons and x or γ rays. These dosimeters suggest application to the measurement of fast neutron beams since their chemical composition is near tissue equivalent. Moreover, their high stability and sensitivity suggest their use for transfer dosimetry by mail among installations conducting radiobiological and clinical research with fast neutrons. Recently these materials have become commercially available, and we have begun preliminary measurements of their neutron response. The dosimeters being tested consist of a 5 mmolar solution of hexa hydroxyethyl pararosanaline cyanide in ethylene glycol monomethyl ether.* In our preliminary trial the solution was irradiated to doses of 1000 rads (tissue) with cobalt 60 γ rays or fast neutrons produced by the $^{9}Be(^{3}He, n)$ reaction using the Institute cyclotron. Dosimeters were read to a precision of ±5% in a Beckman DU spectrophotometer using 1 cm path length cells at 599 nanometers. For cobalt 60 γ rays the observed optical density change upon irradiation was 2.85×10^{-3} ODU/rad for neutrons a value of 2.56×10^{-3} ODU/rad was obtained. The neutron/gamma response ratio is therefore approximately 0.9 ± .05 and further investigations would seem desirable.

C. LET Measurements and Biological Dosimetry

1. LET Distributions

Work reported in our previous progress report (5) on the application of a miniature Rossi type proportional counter** (10, 11) to in-phantom measurements has continued.

As discussed in that report, a major difficulty in obtaining data spanning the entire LET range of interest, (0.1 to 1000 KeV per micron), was due to high amplitude noise pulses generated by the cyclotron magnet power supply. Initial attempts to eliminate this problem by the use of differential amplifiers for common mode rejection or gated delay amplifiers proved unsuccessful. The difficulty was finally overcome by providing an anti-coincidence

---

*Obtained from EG & G, Inc., Goleta, California

**Ibid.

input to the multichannel analyzer from the Silicon Controlled Rectifier driving circuitry of the magnet power supply. This signal inhibits analysis during the SCR firing and effectively reduces the noise level to the point that amplifier noise becomes a significant gain limiting factor.

The accurate accumulation of pulse height spectra covering some 4 decades in amplitude and 5 decades in count rate places stringent demands on the functioning of the electronics in the analysis system. Considerable delays were encountered because of malfunctions in the various available linear amplifiers and multichannel analyzers which had not been evident when the same equipment was employed in γ ray spectroscopy. Moreover, despite extreme care in the determination of the relative gains used in acquiring different segments of a given pulse height spectrum, it was found necessary to develop a computer routine to permit accurate registration of these segments.

A Fortran program has been written for the IBM 1800 Computer, which will handle up to three overlapping spectra of 256 channels each. The program corrects for dead-time losses and normalizes the spectra for quantity of incident radiation. If the relative channel widths between spectra are found to differ from their input values, they are adjusted. The program calculates the functions P(Y), D(Y) and D(L) and these are printed out and plotted on a log-log scale. The necessary adjustment of the relative channel widths between spectra, because of imprecise knowledge of relative gains and baseline offsets, is accomplished in the following manner. Starting with the lowest available channel (highest counts) on the spectrum of larger channel width, the counts are normalized to correspond to the smaller channel width of the other spectrum. A search is made of the second spectrum for two channels containing counts neighboring the normalized value from the first spectrum. An interpolation between these two channels produces the channel number (Y) on the second spectrum equivalent in energy to the channel number (X) of the first spectrum. This process is repeated for successive channels of the first spectrum until the point is reached where the difference in counts between channels is of the order of the inherent scatter. A linear least squares fit of Y to X is performed, whose slope is the adjusted channel width ratio, and whose intercept is the zero offset between the two spectra. The procedure is repeated, using a range of initial values to normalize the counts from the first spectrum, until the agreement between input and calculated ratios reaches the desired level. Convergence is quite rapid. The resulting normalized distributions may then be smoothed by a variety of techniques, and the functions P(Y), D(Y) and D(L) computed, where P(Y) is the probability of an event occurring per unit energy, D(Y) is the dose per unit energy interval and D(L) is the distribution of dose with LET for the particles traversing the counter. These functions are computed according to the following formulas:

$$P(Y)_{I,J} = \frac{C_{I,J}}{E_I \cdot \sum_{I=1}^{N} \sum_{J=JL(I)}^{JU(I)} C_{I,J}}$$

$$D(Y)_{I,J} = \frac{J \cdot C_{I,J}}{\sum_{I=1}^{N} E_I \sum_{J=JL(I)}^{JU(I)} J \cdot C_{I,J}}$$

$$D(L)_{I,J} = \frac{J^2 \left[C_{I,J} - \frac{J}{J+1} C_{I,J} + 1 \right]}{3 \sum_{I=1}^{N} E_I \sum_{J=JL(I)}^{JU(I)} J \cdot C_{I,J}}$$

where I = spectrum number

J = channel number (corrected for zero offset)

N = total number of spectra

JL(I), JU(I) = lower and upper limits of portions of each spectrum employed in the calculation

E_I = KeV/micron/channel in spectrum I

$C_{I,J}$ = number of events (counts) in spectrum I, channel J

The calculation of D(L), or fraction of radiation dose delivered versus LET of ionizing event in a neutron field, involves the analysis of multichannel spectra of frequency versus energy deposition in the detector. If C_n represents the number of events recorded in the nth channel, the measurement D(L) is a function of the quantity $C_n - \frac{n}{n+1} C_n + 1$. Since the measurement is thus a function of the difference between Poisson-distributed variables, when this difference is of the order of the inherent scatter of these variables, the measurement has poor precision. In practice, a spectrum may contain counts ranging over five orders of magnitude, with the result that the precision of the calculated D(L) also varies considerably.

One approach to this problem is the smoothing of the fluctuations in the original spectrum by various numerical algorithms. Among those we have employed are linear, parabolic, exponential, and Gaussian convolutions of the original data. In each case, repeated iterations are performed, until the desired degree of smoothness is obtained. The principal problem with these methods, however,

is that they introduce trends, or systematic deviations between the smoothed and original data sets, which are not statistically justifiable. If the smoothing process is halted before these trends appear, the resulting smoothness is insufficient.

An alternate method for the reduction of noise consists of applying a filter function to the Fourier transform of the original distribution and then taking the inverse transform as the smoothed distribution. For this method to be effective, it is necessary that the amplitudes of the frequency components fall off rapidly with increasing frequency. Because of the large numerical range of our data this is not the case. Even when attempting to smooth the difference between the distribution and an approximating exponential or power function, we found that the amplitudes of the high frequency components fell off insufficiently rapidly.

Another approach underway is the use of the cubic spline method of interpolation for generating a smooth curve between selected points of the distribution (called "knots"). The placement of these knots, however, is critical, and their spacing represents a compromise between the production of trends and the smoothness of the final product.

Finally, it may prove desirable to combine channels of the spectrum, the number summed to increase with increasing channel number (decreasing counts), and represent the measured D(L) as the average for each region.

Although a statistically satisfactory method of smoothing data has not been developed a large number of pulse height spectra have been accumulated for various neutron fields. While comprehensive analysis and radiobiological interpretation of these is being delayed until development of the data smoothing routine is completed, several sample D(L) distributions are shown in Figures II and III.

2. Biological Dosimetry

Our previous progress report (5) discussed briefly the results of Drs. Djordjevic and Evans (12) of this Institute which measured the RBE for fast neutrons from the $^{9}Be(^{3}He, n)$ reaction and also suggested some decrease with depth in a scattering medium. These experiments were performed using monolayers of HeLa cells, and personnel on this contract were involved in the design and dosimetric analysis of this experiment. Similar results have been reported by Berry (13) and Nias and Greene (14) and differ from those obtained by McNally and Bewley (15), who found no dependence of RBE on depth. It is hoped that analysis of the LET measurements discussed earlier will contribute to an understanding of these results.

The original cell system was unsuited to the study of the oxygen enhancement ratio since the cells were plated on the

inner face of a polystyrene culture bottle filled with medium. Some effort was spent in attempting to develop an enclosure for the cells which would provide a suitable radiation environment for the cells and be directly compatible with the geometry of the ion chamber used for dose measurement. This approach was abandoned because it was found that the Shonka A-150 plastic, of which the enclosure was fabricated released a substance toxic to the cells. A new method of handling the HeLa cells has been developed by Dr. Djordjevic. The cells are clumped with either non-metabolizing or metabolizing but non-reproductively competent feeder cells. In the latter case the HeLa cells are rendered chronically hypoxic because of the oxygen consumption by the feeder cells. This system which retains cell viability for long periods of time is particularly suited for the low dose rates experienced using ^{252}Cf spontaneous fission sources. Preliminary measurements for which dosimetry was performed indicate an OER of approximately 1.6 for neutrons from the ^{9}Be(^{3}He, n) reaction at 2.4 cm depth in water and 3.2 for ^{60}Co γ rays under similar conditions.

Dose measurements have recently been initiated for the ^{252}Cf spontaneous fission sources in cooperation with Dr. Lowell Anderson of Memorial Hospital. Measurements are being performed in a solid phantom of 6/6 nylon. This material has been found (16) to be indistinguishable from Shonka A-150 tissue equivalent plastic for ion chamber measurements with fast neutrons. The phantom is a 25 cm cube with provision for measurements in 1 cm increments at distances of 1-5 cm from the source axis throughout one quadrant. Ion chambers of about 0.05 cm^{3} collecting volume are employed, a chamber with tissue equivalent plastic walls and tissue equivalent gas for the total dose measurement and a chamber with aluminum walls and argon gas for the gamma ray dose measurement. Extreme care is required to minimize background current, since the currents to be measured are as low as 2-3 x 10^{-15} amp. Preliminary results of total absorbed dose measurements appear to agree closely with earlier measurements by Fairchild (17). Figure IV compares our results with those from references (17, 18, 19).

The ion chambers fabricated for the ^{252}Cf measurements have also been employed for in phantom measurements to determine the dose for studies of the effect of neutron irradiation on reproductive capacity of the female rat, being carried out be Dr. Eric Hahn of the Radiotherapy Research Division. Whole-body exposure to x or γ rays (100-600 R) 3-5 days prior to mating effects a significant increase in the number of ova shed leading subsequently to an increase in implantations and term litter size. However, if the animals are irradiated 12 hours or less prior to mating or during pregnancy, increased embryonic and fetal mortality ensues. The degree of the aforementioned effects are dose dependent. The purpose of these studies is to compare and evaluate the relative effects of neutrons on these parameters. The animals are irradiated at specific times before or during pregnancy, and the numbers of ovulations, implantations and live and dead fetuses are recorded at term pregnancy.

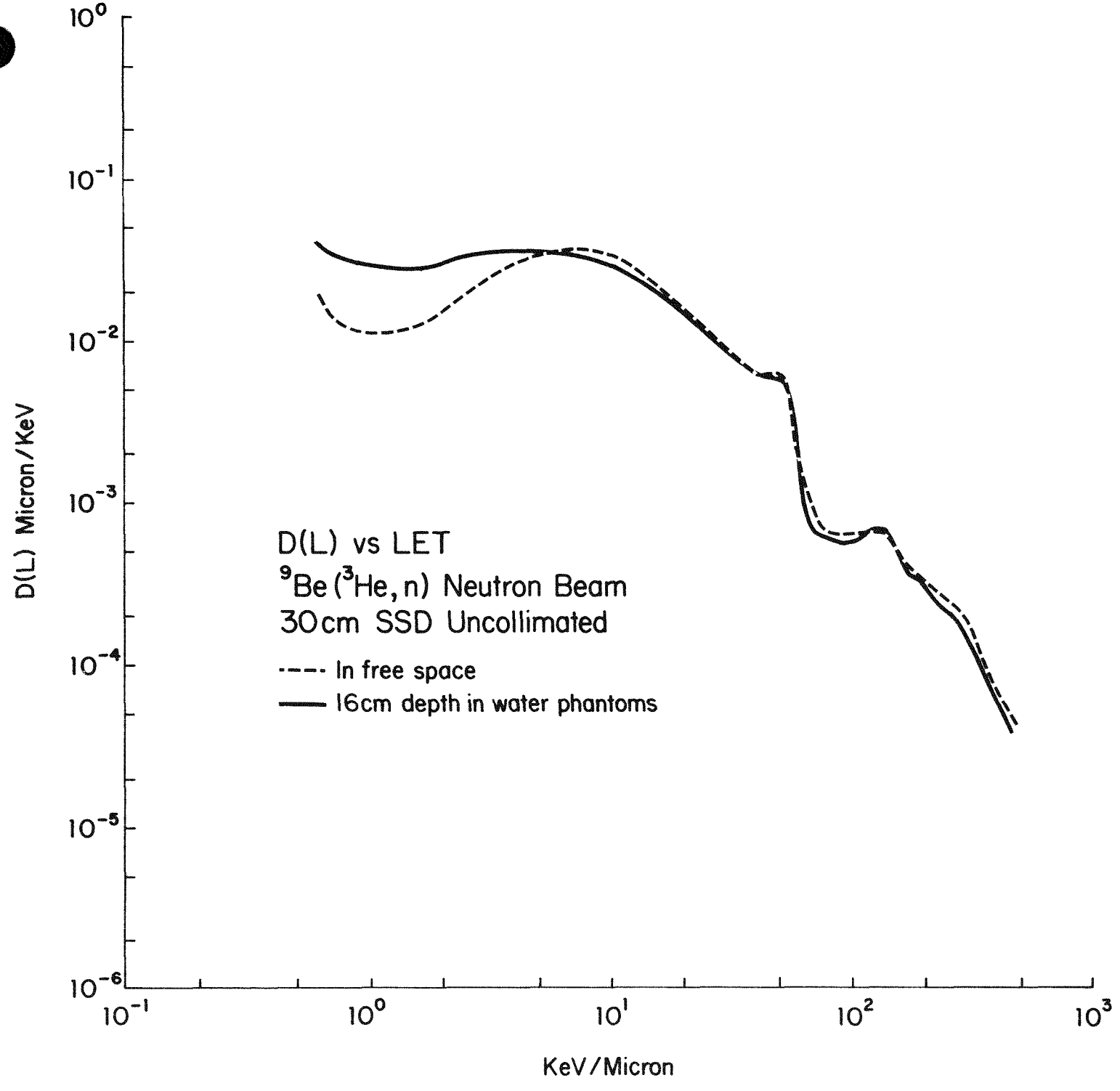
D(L) vs LET
$^{9}Be(^{3}He,n)$ Neutron Beam
30cm SSD Uncollimated
---- In free space
—— 16cm depth in water phantoms
D(L) Micron/KeV
KeV/Micron
10^{0}
10^{-1}
10^{-2}
10^{-3}
10^{-4}
10^{-5}
10^{-6}
10^{-1}
10^{0}
10^{1}
10^{2}
10^{3}

Fig. II

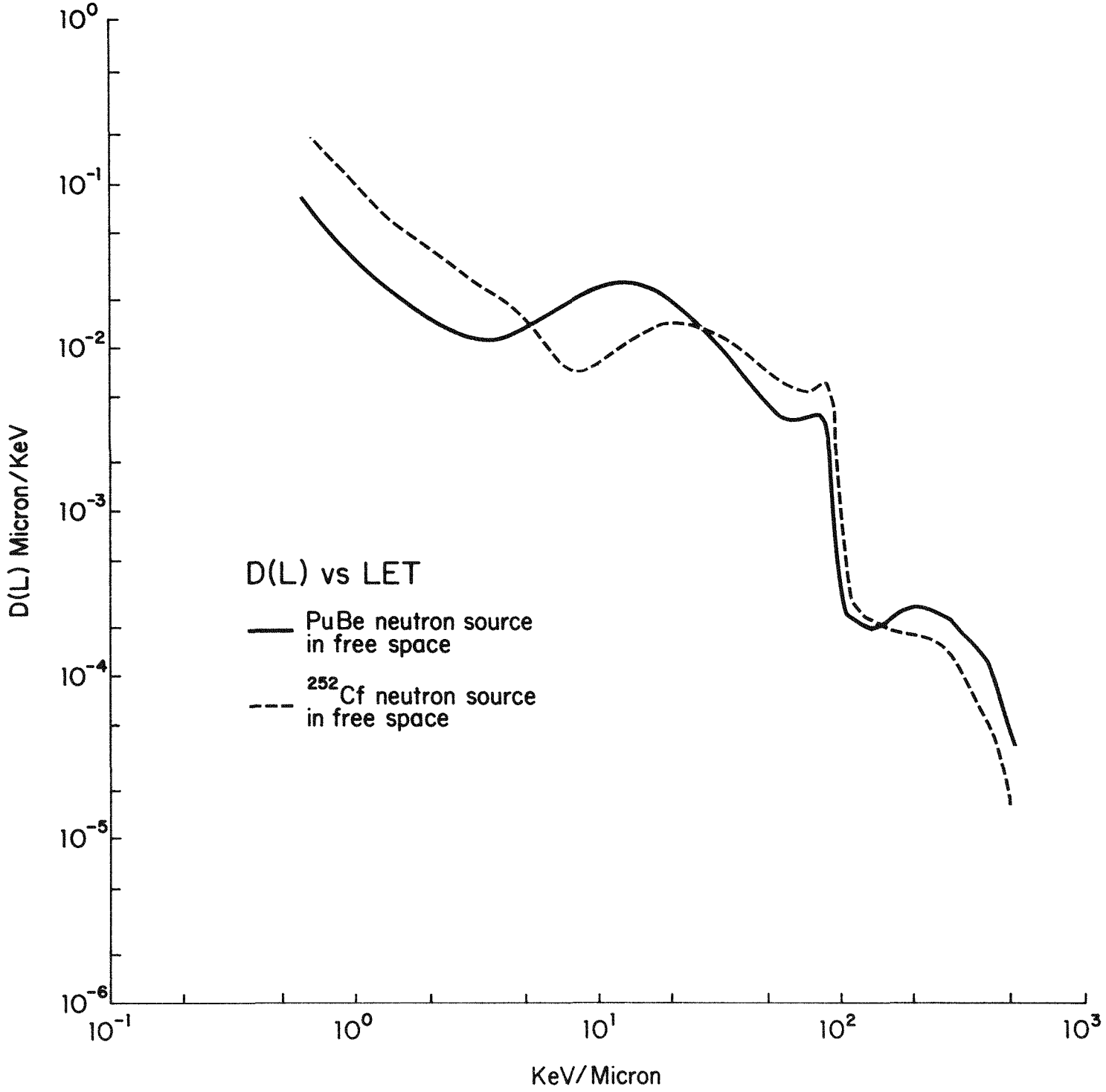
D(L) vs LET
PuBe neutron source in free space
252Cf neutron source in free space
D(L) Micron/KeV
KeV/Micron
10^0
10^-1
10^-2
10^-3
10^-4
10^-5
10^-6
10^-1
10^0
10^1
10^2
10^3

Fig. III

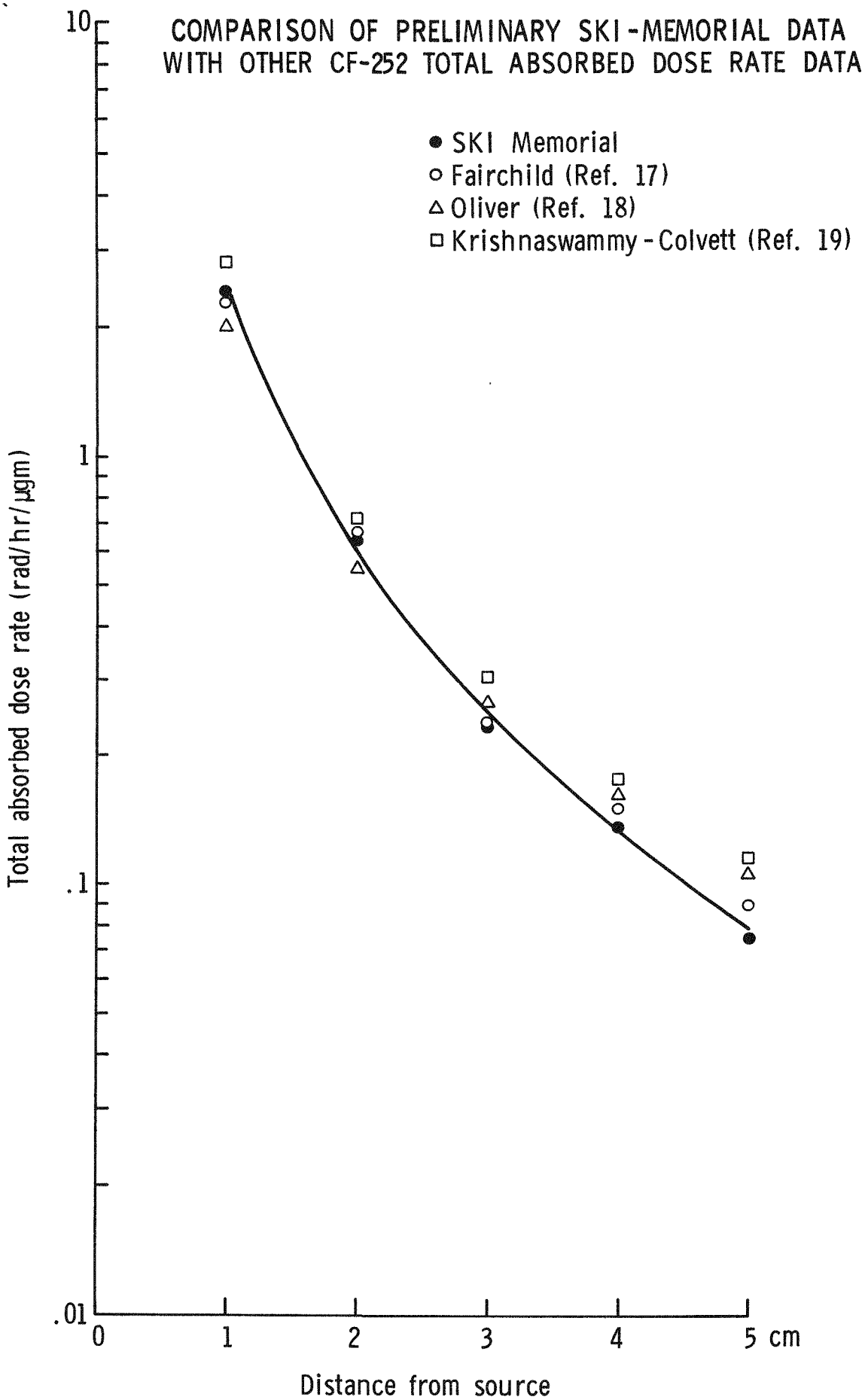
COMPARISON OF PRELIMINARY SKI-MEMORIAL DATA
WITH OTHER CF-252 TOTAL ABSORBED DOSE RATE DATA
SKI Memorial
Fairchild (Ref. 17)
Oliver (Ref. 18)
Krishnaswammy-Colvett (Ref. 19)
Total absorbed dose rate (rad/hr/µgm)
10
1
.1
.01
0
1
2
3
4
5 cm
Distance from source

Fig. IV

III. DOSIMETRY OF ULTRA-HIGH INTENSITY ELECTRON SOURCES

A. Introduction

The high intensity pulsed electron generators at this laboratory are employed in cellular radiobiological experiments and dosimetric studies at ultra-high dose rates. Current radiobiological experiments involve measurements of the radiosensitivity of bacterial and mammalian cells exposed to single (20) and double pulses (21) of electrons in an atmosphere of controlled oxygen concentration. Techniques have been developed for irradiating and assaying bacterial cells in the form of a thin layer deposited on a Millipore filter. This arrangement allows for the rapid exchange of oxygen. In order to study the effect of oxygen on the radiosensitivity of cellular organisms, the absorbed dose must be accurately measured. The use of thin plastic scintillators provides a method whereby the dose delivered to a thin cellular layer can be determined.

B. Description of Electron Generators

The electron generators are commercially available units which produce singly occurring pulses of electrons by field emission. The electrons emerge through a 0.025 mm thick titanium window which results in a root-mean-square angle of scattering of about 22^{o} (22) measured from the beam axis for 500 KeV electrons. Although the window is thin enough to cause only a small amount of absorption, there is still considerable angular scattering so that the beam spreads out rapidly as it emerges. The electron current pulse duration is 3 nanoseconds at the half maximum points, and the average beam current in the pulse is about 4000 amperes. The maximum electron energy is approximately 500 KeV as measured by the linearly extrapolated range of the beam in an aluminum absorber. Doses as high as several megarads per pulse can be delivered near the tube window so that dose rates can be in excess of 10^{14} rads/second.

C. Experimental Techniques

It was expected that the dose versus depth distribution for the electron beam would have a build-up of dose from the irradiated surface of a tissue-like sample to a maximum at a point where electronic equilibrium is achieved. Previous measurements (23) have shown that a similar electron beam, with a pulse duration of 30 nanoseconds, can produce a steeply rising depth-dose distribution in polystyrene such that the dose at a depth of 40 mg/cm^2 is approximately 35% greater than the surface dose. The possibility of a large dose gradient near the irradiated surface suggested the use of an extrapolation experiment in which the detector thickness is varied.

Figure V (a) shows four views of the detector which is

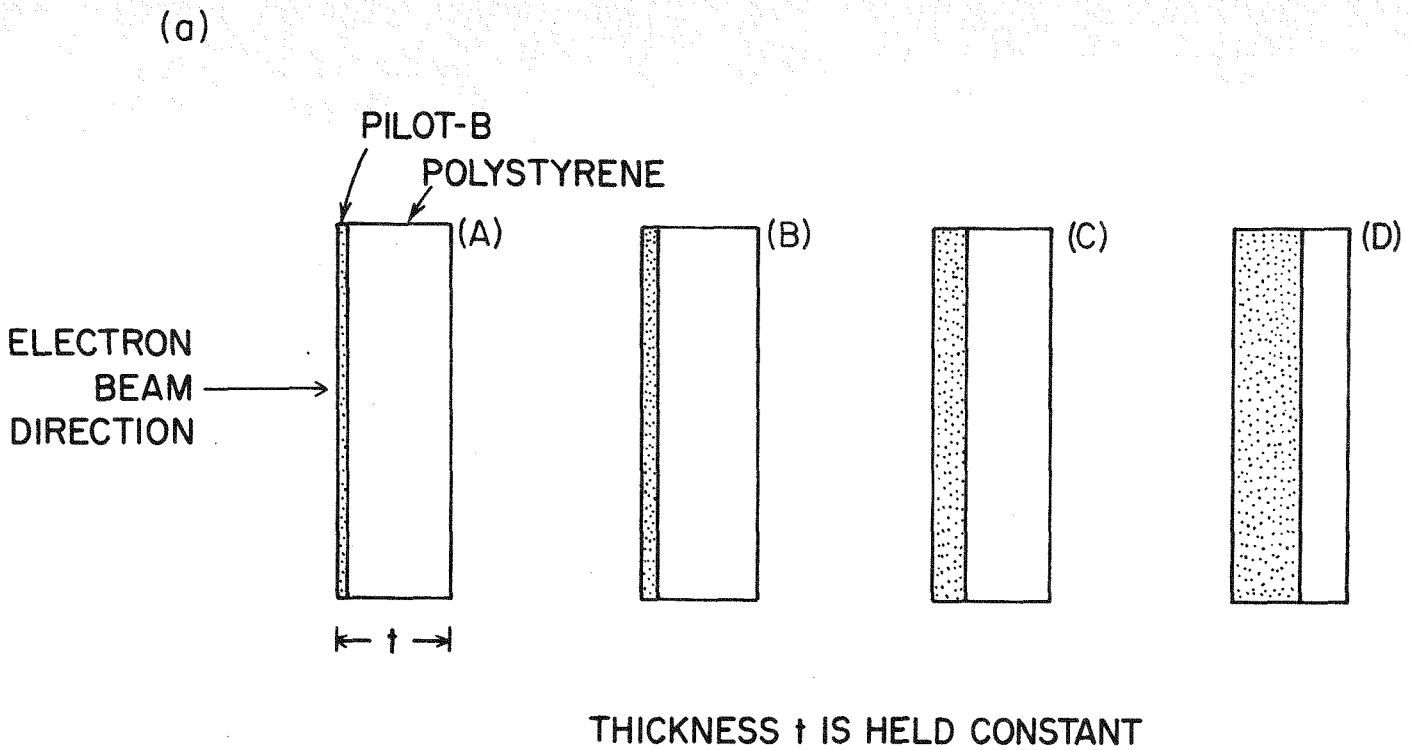

Fig. V. Arrangement of scintillators for extrapolation and depth-dose measurements.

placed at the irradiation position normally occupied by a biological sample. View (A) shows the thinnest commercially available disk of Pilot-B scintillator (0.015 mm measured thickness) with a backing of transparent polystyrene such that the combined thickness is approximately equal to the total thickness of a wet cellular layer plus the Millipore filter on which the cells rest (0.17 mm). Views (B) through (D) show how the scintillator thickness was increased while the total thickness was held constant. The scintillator light output can be calibrated in terms of rads by using a thin foil calorimeter which will be discussed in a subsequent paragraph. Figure V (b) shows the arrangement used for depth dose measurements.

D. Scintillation Detector System

Figure VI shows a block diagram of the experimental arrangement. The space between the electron generator appearing at the left and the detector is evacuated to a pressure of about 10^{-3} Torr. Different length aluminum drift tubes can be used to vary the dose delivered to the detector since the electron generator has a fixed output per pulse. Evacuating the space between source and experiment eliminates beam instabilities resulting from the "pinch" effect (24) which occurs when the beam is fired into air. This effect is due to ionization of the air by the electron beam where the secondary electrons migrate out and a net positive charge causes a magnetic refocusing of the diverging primary electron beam.

The pickup loop serves as the sensing element for a non-intercepting electron beam monitor which can detect pulse to pulse fluctuations in the output of the electron beam since series of individual pulses delivered by the source and recorded with either a faraday cup or a calorimeter will typically show a root-mean-square variation of ±4.5% with maximum to minimum variations of ±10%. This loop is operated as a current transformer producing a voltage pulse which is induced by the magnetic field associated with the electron bunch moving over the loop area. The monitor system was developed in this laboratory and has been described elsewhere (25). There are two 0.051 mm thick Mylar windows between the source and detector. The effect of this material on our measurements will be discussed in a subsequent paragraph dealing with the depth dose distribution.

The light pulse that results when electrons irradiate the Pilot-B scintillator disk is viewed with an ITT model FW-114 photodiode whose rise time is 0.5 nanoseconds when the diode is operated at -2100 volts. Since the detector thickness is less than the range of the electrons a disk of transparent polystyrene 3.18 mm thick was used to prevent electrons from hitting the phototube. The optical transmission of the polystyrene, measured with a Beckman spectrophotometer, indicated that the photodiode was recording only the main peak (400 nanometers) in the fluorescence spectrum of the Pilot-B scintillator. A neutral density filter

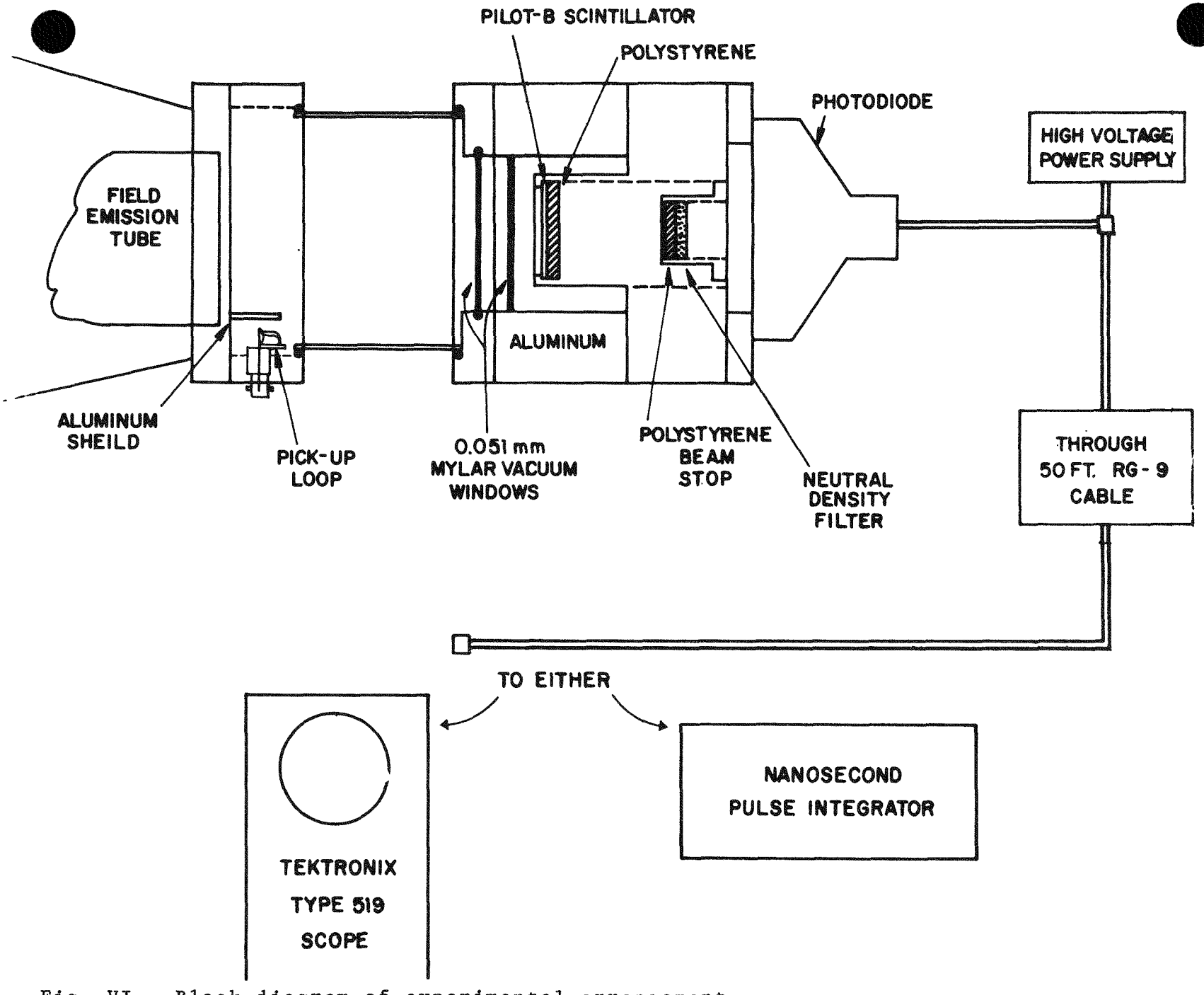

Fig. VI. Block diagram of experimental arrangement

was used to control the intensity of the scintillator light pulse when the source to experiment distance was small. The distance between the scintillator disk and the beam stop was large enough so that backscatter was negligible. The output of the phototube can be viewed with a Tektronix type 519 oscilloscope whose rise time is less than 0.35 nanoseconds, or recorded by using a nanosecond pulse integrator which measures the area under the pulse produced by the phototube.

Figure VII (a) shows the voltage waveform from a faraday cup which can be placed at the irradiation position in the same manner as the scintillation detector. The time-scale is 5 nanoseconds/division and the full width at half the maximum pulse height is approximately 3 nanoseconds. Figure VII (b) shows the output of the photodiode which is viewing the scintillator light pulse. The time-scale is again 5 nanoseconds/division and the broadening of the pulse is due to the decay time of the Pilot-B scintillator which is about 2 nanoseconds.

E. Dose Rate Dependence of Pilot-B

The light output for various thicknesses of Pilot-B scintillator was measured as a function of source to detector distance. Figure VIII shows the area under the pulse produced by the phototube (measured in units of coulombs) as a function of the distance from the source for the thin scintillator disks used in the extrapolation experiments and depth-dose measurements. Least squares analyses of the data indicate a power law dependence with an exponent of approximately -2.3 for each of the scintillators used. The same dependence with distance is found using a faraday cup. The fall off with distance which is somewhat faster than $1/r^2$ is apparently due to beam divergence previously mentioned in the description of the electron generators.

The absorbed dose delivered to the Pilot-B disks was measured with a thin foil calorimeter. Since the time duration of the pulse is known, the dose rate (rads/second) can be computed. Experimental results are shown in Figure IX for the 0.112 mm thick Pilot-B disk. The solid line through the data points is the result of a least squares fit which indicates a slope of 0.94. The scintillator light output shows no saturation from 8.5×10^{10} up to 2.4×10^{13} rads/second. During the course of these experiments there was apparently no change in the sensitivity of the Pilot-B scintillators after exposure to several hundred electron pulses which corresponds to a total dose of several megarads.

F. Results of Extrapolation and Depth Dose Measurements

Figure X shows the result of measuring the light output of four different thickness Pilot-B scintillators in the geometry shown in Figure V (a). The measured output is expressed in rads and plotted as a function of the scintillator thickness. A linear least squares fit of the data indicates a lack of build-up. The

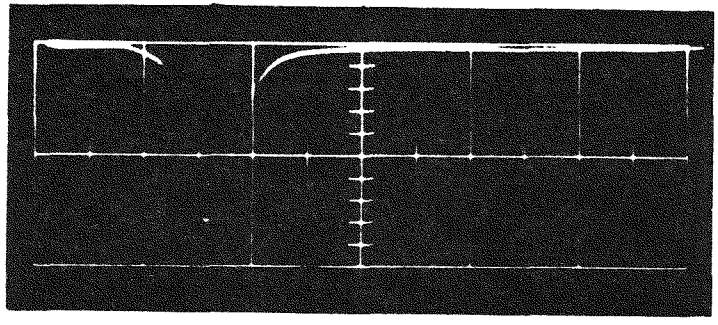

(a) ELECTRON CURRENT PULSE VIEWED BY FARADAY CUP (5NS/DIV)

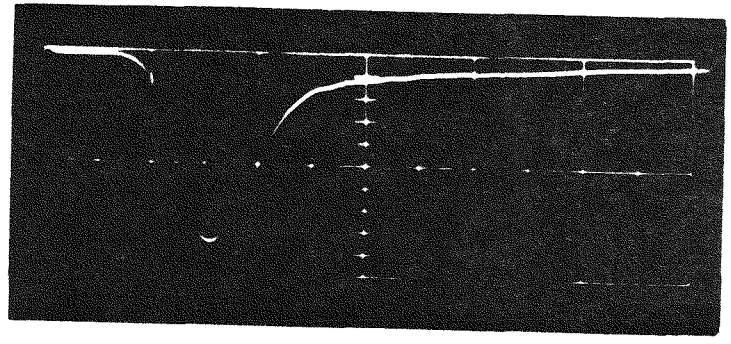

(b) SCINTILLATOR LIGHT OUTPUT PULSE VIEWED BY PHOTODIODE (5NS/DIV)

Fig. VII. Voltage waveforms produced by a faraday cup and a photodiode viewing a Pilot - B scintillator light pulse.

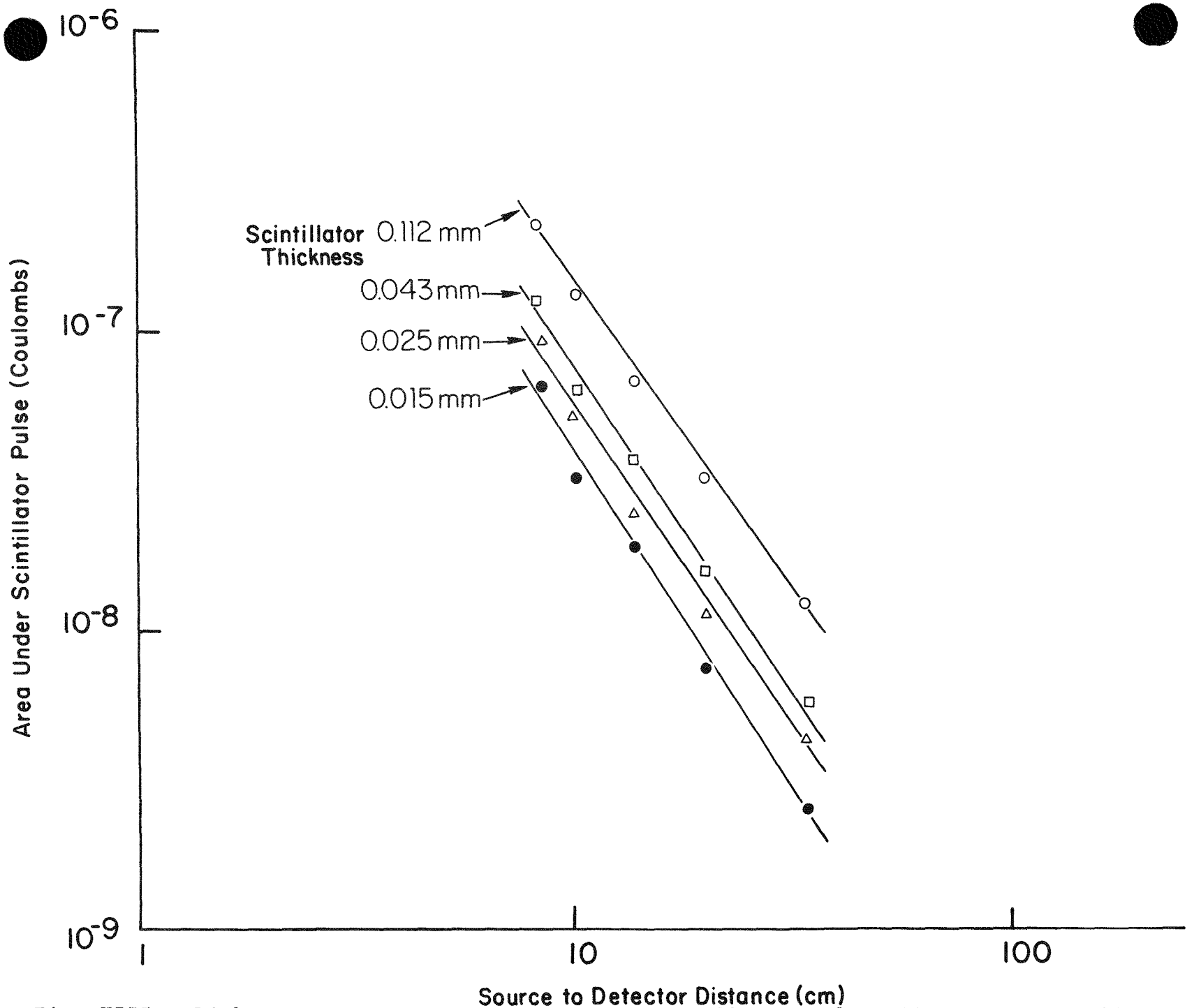

Fig. VIII. Light output versus source to detector distance for Pilot - B scintillators of different thicknesses.

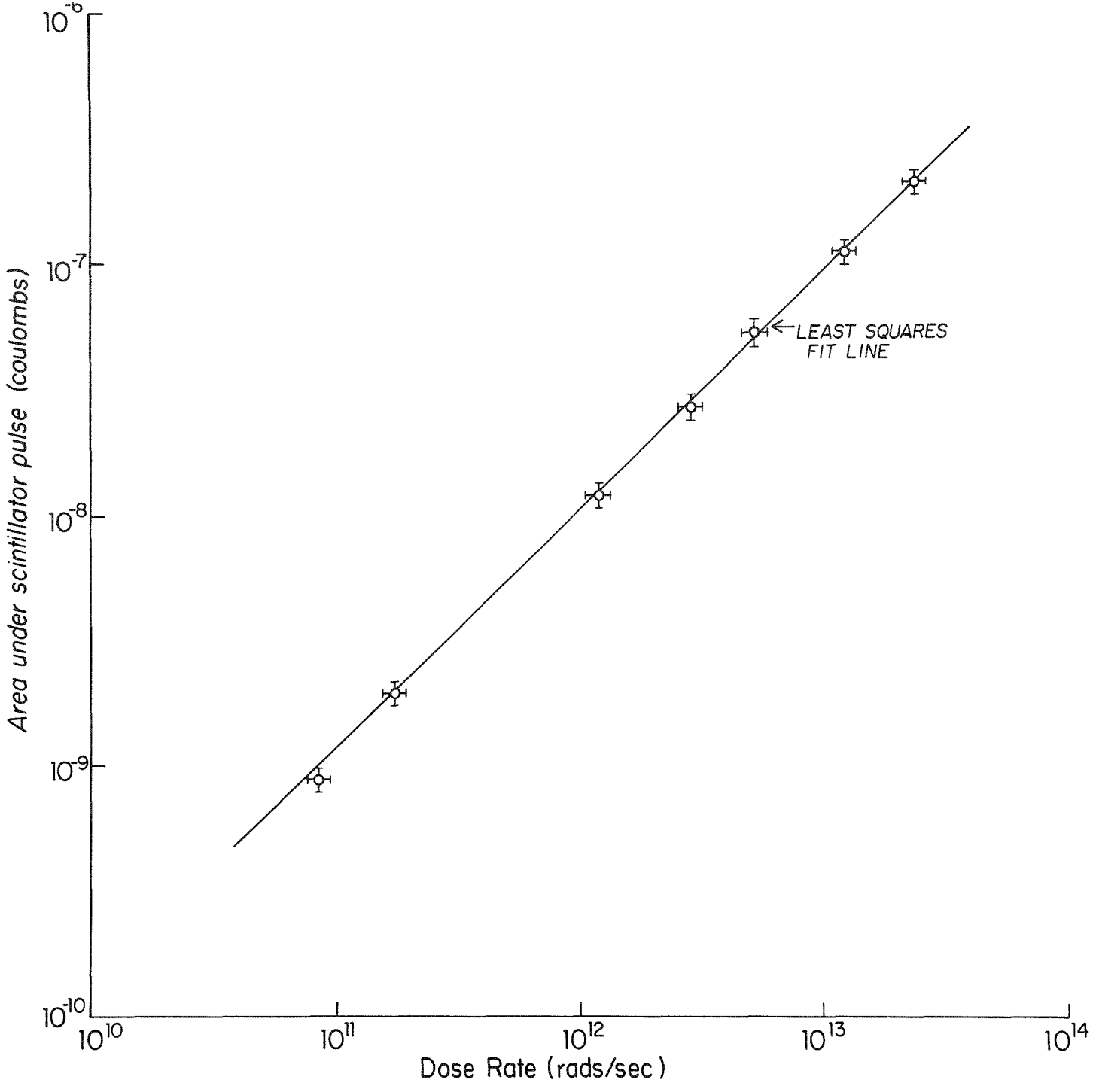

Fig. IX. Dose rate dependence of scintillator light output

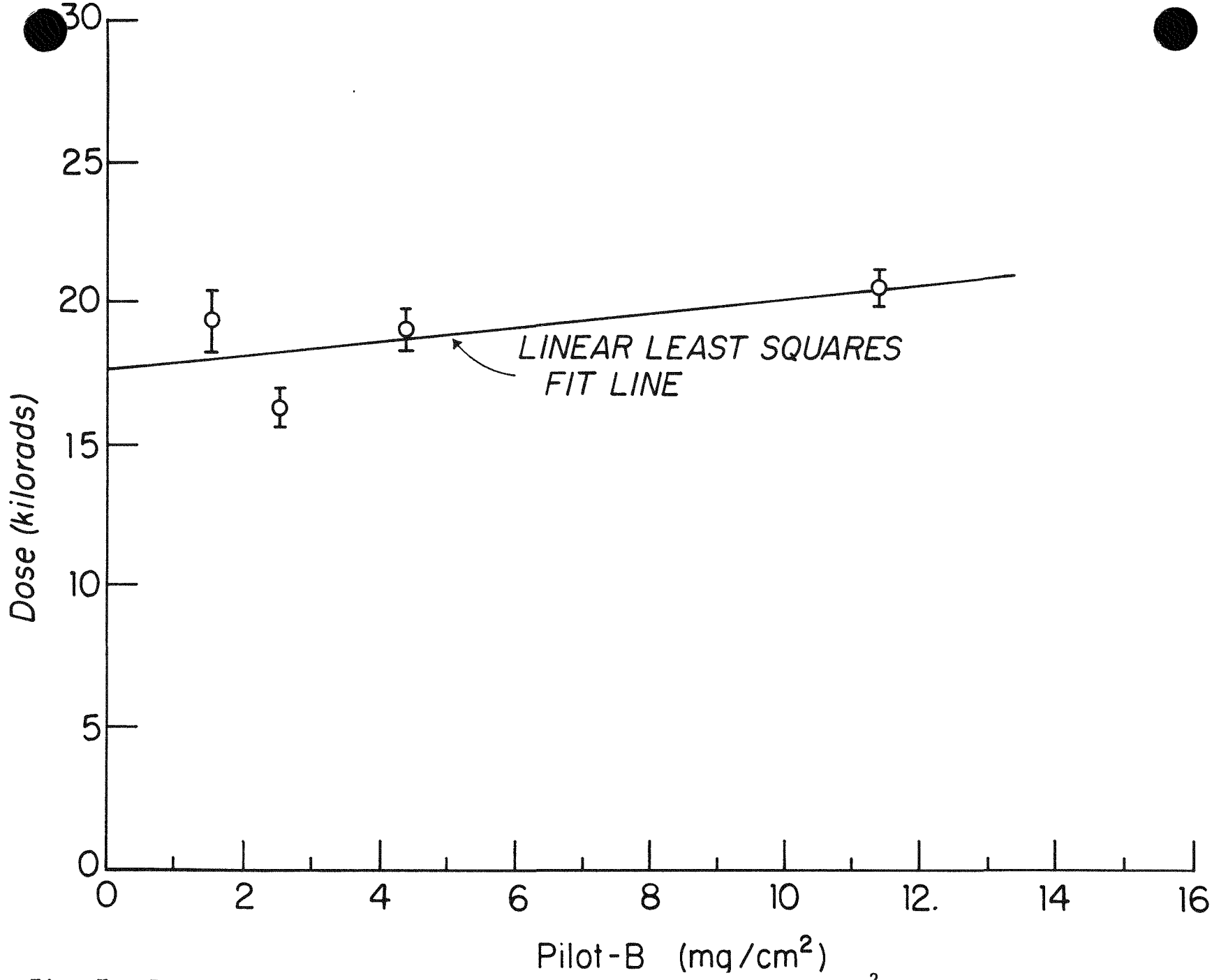

Fig. X. Dose versus scintillator thickness (expressed in mg/cm^2)

y intercept shows that the dose at the surface is approximately 18 kilorads. Figure XI shows the depth dose distribution in polystyrene which was obtained at the same source to detector distance using a 0.015 mm thick disk of Pilot-B scintillator. Both of these experiments were performed for source to detector distances ranging from 8.3 cm to 28 cm and similar results were obtained. Since no appreciable build-up was measured at any of these distances, the calculation of absorbed dose is simplified by the lack of a dose gradient. A possible explanation for the absence of a build up is the presence of low energy electrons in the beam which reaches the experiment. These low energy secondary electrons can be generated in the two Mylar windows which are close to the detector, and some scattering might result from the walls of the aluminum drift tubes (refer to Figure VI).

G. Electron Beam Transmission Measurements

The two Mylar windows do not cause appreciable absorption of the electron beam, but they do contribute low energy secondary electrons to the beam which reaches the sample. An attempt to analyze the electron beam in our experimental geometry was made by placing disks of aluminum, ranging in thickness from 0.13 mm to 0.78 mm, in front of a faraday cup. Figure XII shows the number of electrons transmitted expressed as a percent of the number incident and plotted versus the aluminum thickness. The solid curves have been obtained from data for mono-energetic electrons (26). It can be seen that the maximum energy is about 500 KeV, but the attenuation in the first 30 mg/cm^2 indicates the presence of lower energies. These data imply that a simple estimation of the absorbed dose delivered to a water layer a few microns in thickness cannot be made by measuring the number of electrons which would be incident and using the value for the stopping power of 500 KeV electrons. This estimate would be about a factor of two lower than the direct measurement by calorimetry. The aluminum foil transmission method of examining the spectrum of the electron beam is admittedly crude and further investigations are planned which include the construction of a magnetic spectrometer.

H. Thin Foil Calorimeter

A direct measurement of absorbed dose was made with a calorimeter which is shown in Figure XIII. The calorimeter enclosure, the scintillator holder, and the faraday cup were constructed so that they would be irradiated in the same geometry as a biological sample. The calorimeter absorber is a 2.54 cm diameter disk of beryllium 0.025 mm thick. The temperature rise in the disk is measured using a miniature iron-constantan thermocouple with an electronic reference junction which provides readings with respect to 0°C. The output of the thermocouple is amplified by a microvolt meter and displayed on an x-y recorder. A typical voltage pulse will exhibit a fast rise in temperature to a peak followed by an exponential decay as the disk cools. The peak temperature rise is determined by extrapolating the cooling curve

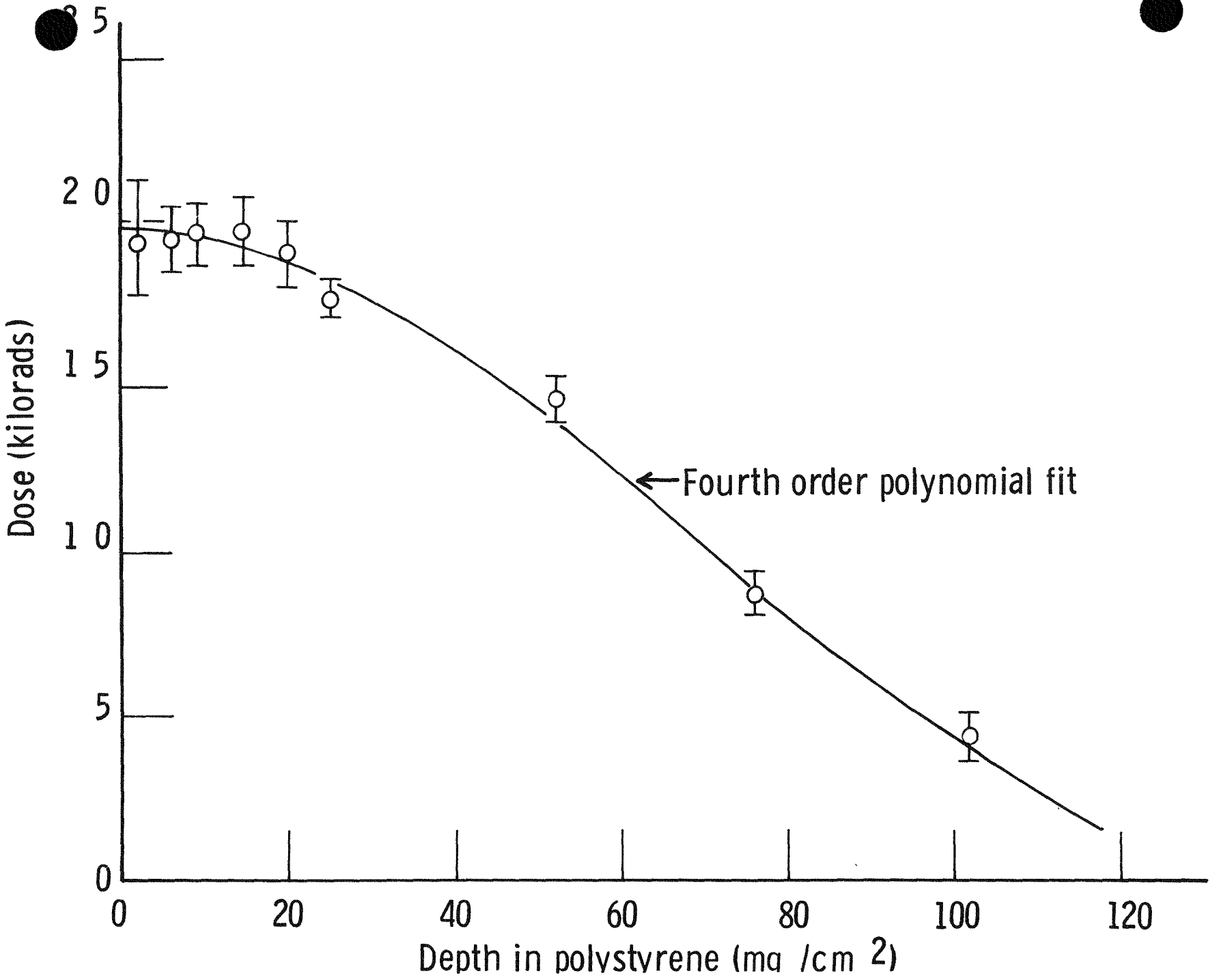

Fig. XI. Depth-dose distribution in polystyrene

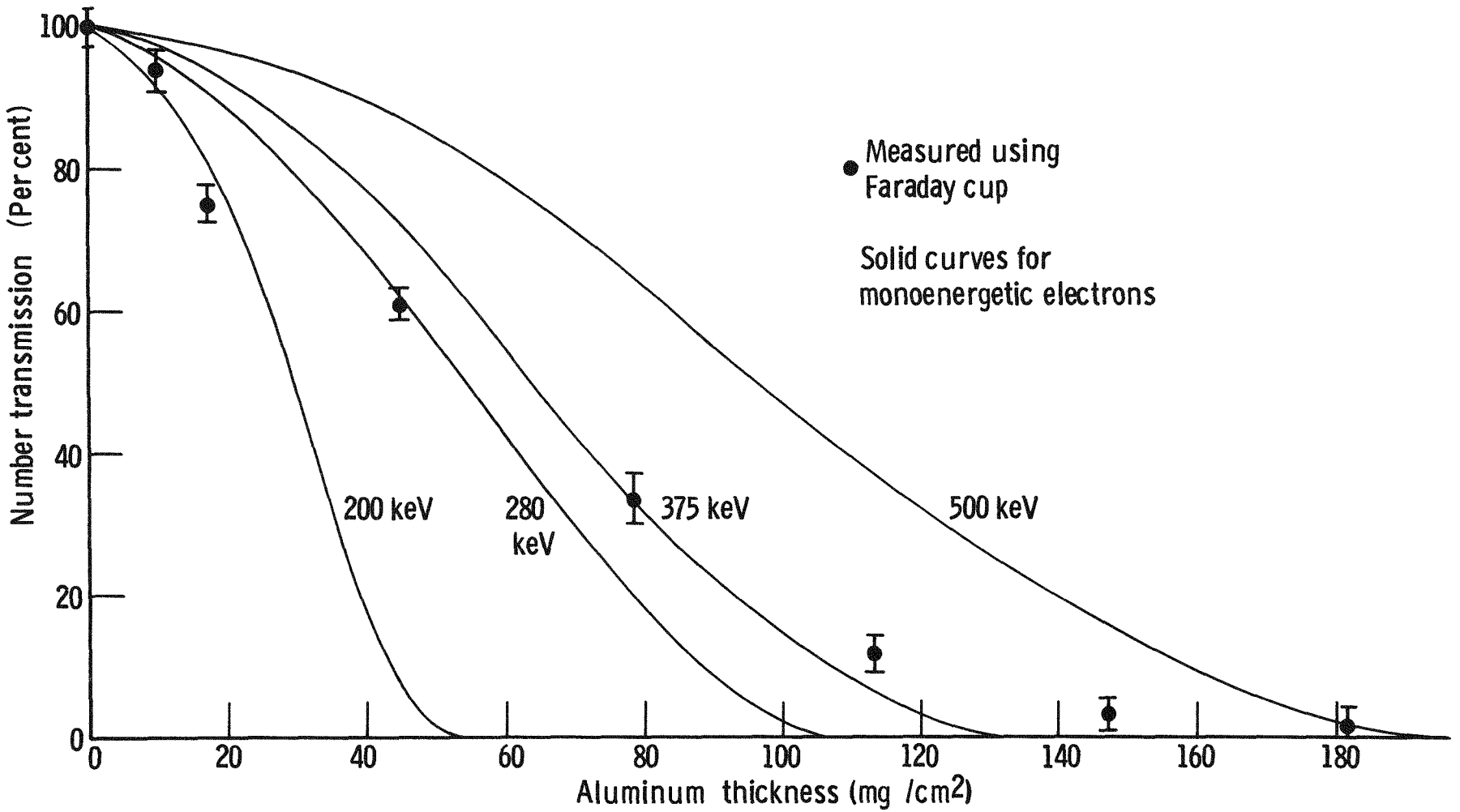

Fig. XII. Electron beam transmission through aluminum

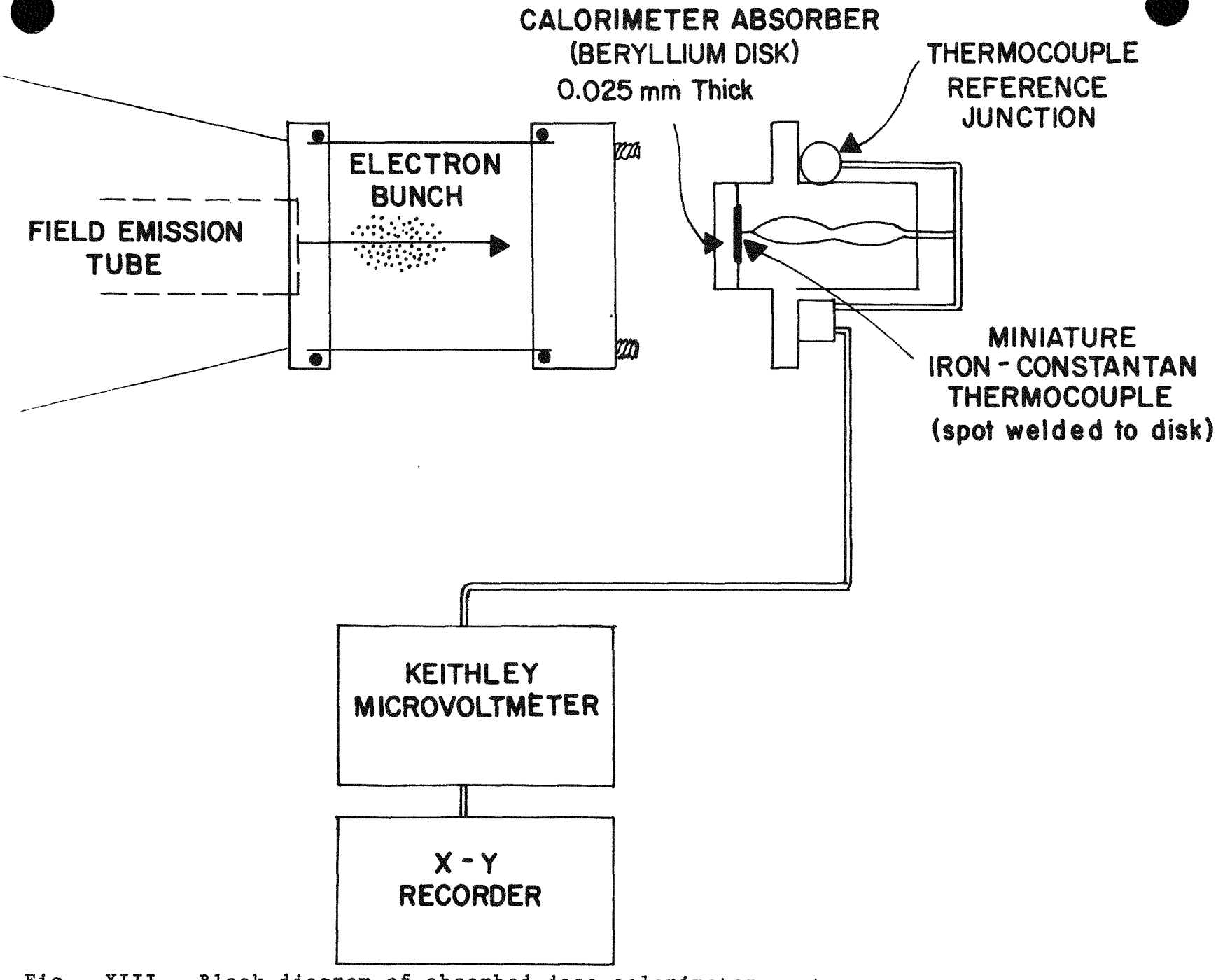

Fig. XIII. Block diagram of absorbed dose calorimeter system

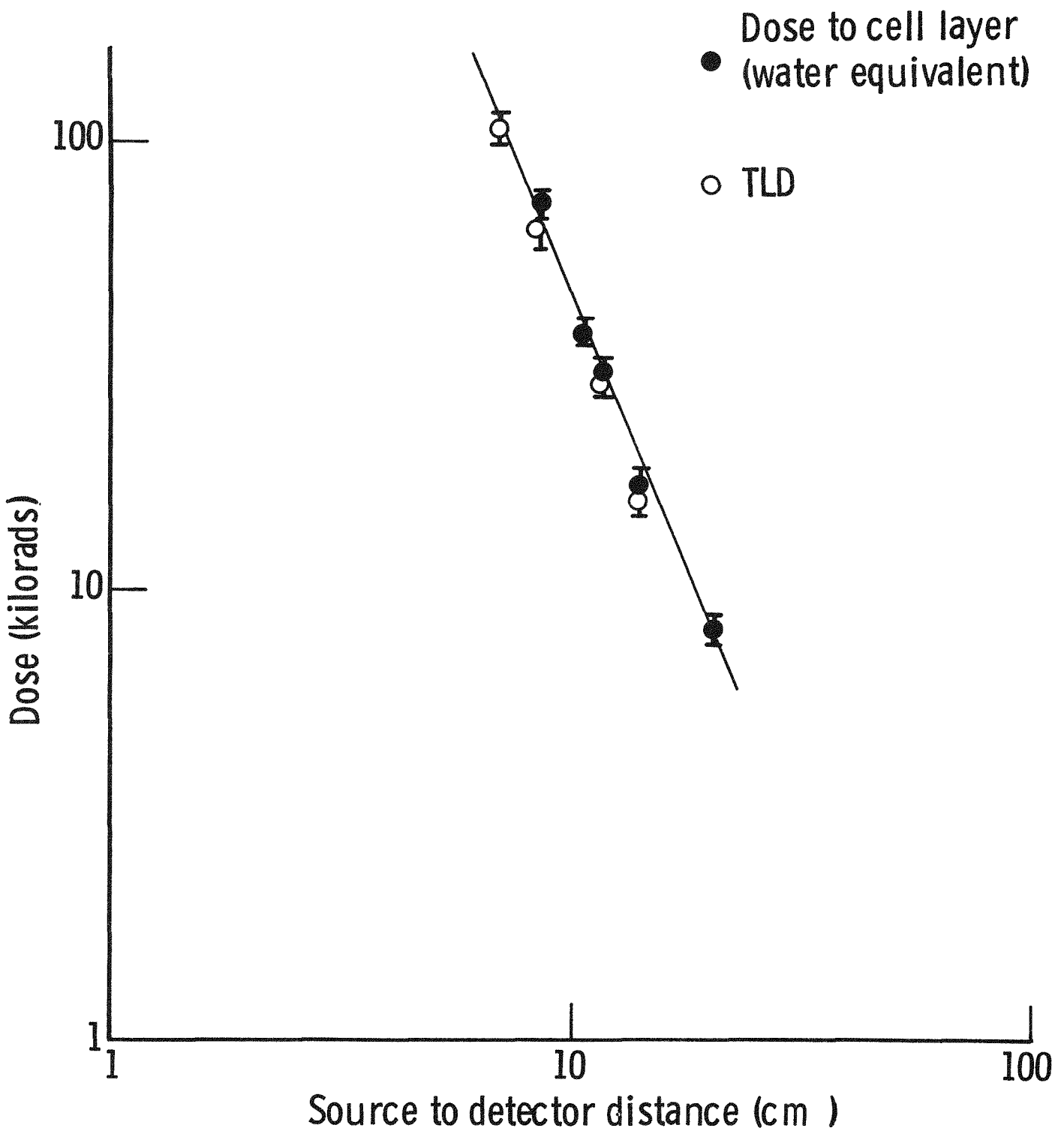

Fig. XIV. Dose delivered to a cell layer as a function of source to detector distance.

back to time t = 0. The specific heat of beryllium is known and the temperature rise is measured; therefore, the quantity of absorbed energy can be determined per gram by using the definition of specific heat. The measured number of calories per gram yields the absorbed dose in beryllium in units of rads.

The extrapolation experiments and depth-dose measurements show an absence of dose build-up near the surface so that the absorbed dose in a cell layer,which can be approximated by water, is given by the absorbed dose in beryllium multiplied by the stopping power ratio of water to beryllium. This ratio as determined from tables provided by the N.B.S. (27) has a constant value of 1.24±1% for electron energies up to 1 MeV.

Figure XIV shows a comparison of the absorbed dose in a cell layer for several source to detector distances, and measurements made with 0.13 mm thick CaF_2: Mn Teflon thermoluminescent dosimeter disks at similar distances. These dosimeters were calibrated by exposure to Cobalt 60 gamma rays at an equilibrium depth in polystyrene. For source to detector distances greater than about 25 cm, the thin foil calorimeter signal to noise ratio becomes small and makes measurements increasingly difficult. In order to extend the range of useful measurement, the scintillator system, for which a calibration factor of light output per rad is known, is used as a secondary dosimeter to determine the absorbed dose delivered to a cell layer at distances which approach 100 cm.

The set of experiments which has been described demonstrate the suitability of using fast response plastic scintillators together with a thin foil calorimeter for determining the dose delivered to a biological specimen. Willis, et al. (28) have performed a calorimetric extrapolation experiment with beryllium absorbers ranging in thickness from 0.100 mm to 0.594 mm irradiated with a Model 706 Febetron. However, a calorimetric extrapolation technique is limited, by signal to noise ratio, to the high dose region near the electron tube face. The dynamic range of the Pilot-B scintillators is such that experiments can be easily performed for dose levels of a few hundred rads. In our experimental geometry the lack of a sharp dose gradient makes the measurement of the dose delivered to a cell layer somewhat easier, but if there had been a build-up then, the technique of extrapolation could have been used to predict the dose absorbed in a layer of a few microns thickness. These dosimetric techniques may be applicable for other pulsed radiation sources, and an absorbed dose monitor could be developed since a thin sheet of Pilot-B can be inserted near the sample without causing much attenuation of the useful beam.

IV. SOLID STATE DETECTOR PROGRAM

A. Germanium Gamma Camera

During the period covered by the report, experimental work has continued towards the construction of a germanium semi - conductor gamma camera. This device is based upon a two dimensional array of detectors which incorporates the orthogonal strip geometry reported previously (23) and shown for convenience of reference in figure XV.

1. Detector Fabrication

Both the conventional lithium drifted germanium diodes and diodes fabricated from recently available ultra pure germanium were tested during this period.

Three germanium slices from three distinct ingots* were lithium drifted for possible formation into an orthogonal strip matrix. Of these, one from crystal number 97309 (the first of the three lithium drifted units processed) had been found satisfactory previous to the last report and was mentioned as ready for formation into a matrix. However, this diode's characteristics degenerated subsequently after it was brought up to room temperature for a short period and the device had to be reprocessed. The diode's properties were eventually recovered sufficiently to warrant an attempt at formation of a matrix. Unfortunately, hairline cracks developed in the diode in the process of cutting the matrix grooves on the surface grinder and the diode had to be discarded.

Each of two other pieces of germanium from two different ingots were drifted to depths of over 6 mm. Because of the availability of ultra-pure germanium at the completion of the drifting of these devices, it was decided to suspend work on these units for the sake of hastening results with ultra-pure germanium.

An important reason for preferring ultra-pure germanium over the lithium drifted diode in a gamma camera is that it eliminates the necessity of meeting a critical time table following completion of the lithium drift in the construction of the matrix geometry. The reason for the need to hurry once a suitable diode is made is because of the tendency of the intrinsic region of these devices to lose compensation rather quickly while at room temperature. While it is possible, in principle, to "flatten" the lithium distribution again after the matrix fabrication, it was thought that the difficulties associated with this procedure and the constant vulnerability of the compensated region to thermal effects were better avoided with the opportunity to do so at hand. In fact the elimination of these shortcomings was considered a major step in making the construction of the large area gamma camera a feasible undertaking.

---

*Nucleonic Products Co., Inc., Canoga Park, California

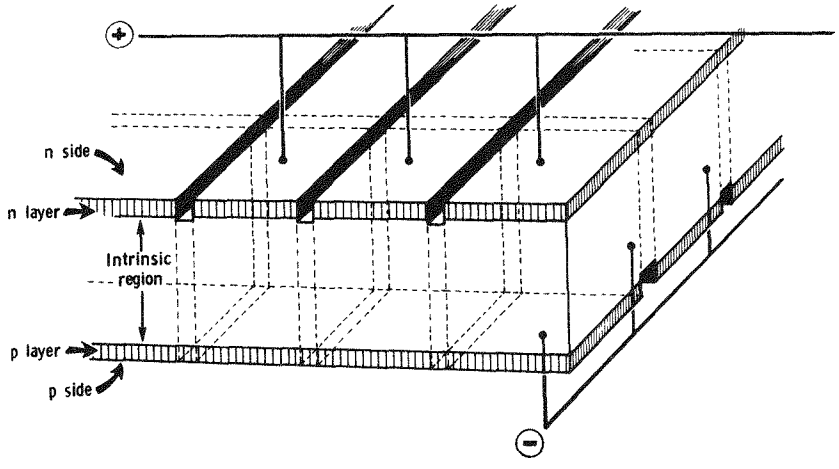

Fig. XV Orthogonal Strip Geometry

The ultra-pure germanium diode on the other hand, while it shares certain problems with the drifted devices as well as having problems peculiar to itself, (e.g., susceptibility to copper "poisoning" at elevated temperature) has stable diode bulk properties not affected by prolonged exposure to room temperature (29).

A 5 mm thick approximately 2.5 cm max. diameter slice of ultra-pure p-type germanium from crystal number 402 was obtained from General Electric Research and Development Laboratory with a specified impurity concentration of $3 \times 10^{10}/cm^3$.* The diode construction was facilitated by J. Llacer of the instrumentation group at Brookhaven National Laboratories who used already existing apparatus to apply a gallium-indium p^+ contact. Further processing of the diode was completed at Sloan Kettering Institute. The n^+ region of the diode is the familiar lithium diffused layer, the thickness in this case being around 200 microns.

Capacitance versus reverse bias, and leakage current versus reverse bias measurements were made after cutting the diode into a (1.8 x 1.26) cm rectangle and following chemical etching. These data are shown in figures XVI.

The C-V measurements were repeated and again led to an impurity concentration of around $5.5 \times 10^{10}/cm^3$ although the supplier's data indicated a figure of $3 \times 10^{10}/cm^3$. Since no heating of the diode above 370°C had occurred and since the total time above 350°C was not more than a couple of minutes, it was not possible to attribute the discrepancy to copper diffusion. Although the frequent ambiguity of capacitance measurements is well recognized, the reproducibility of the data between consecutive surface treatments and the flattening of the capacitance values at the expected theoretical voltage appropriate to the known diode thickness for the higher figure of impurity concentration suggest that the impurity concentration figure actually may be as high as $5 \times 10^{10}/cm^3$.

Spectral measurements were made with this diode for Co 60 and Co 57 gamma rays. The best value of resolution obtained for Co 60 was 2.8 KeV (FWHM) at a bias voltage above 500 volts. At a lower bias voltage pulse height loss became evident and the peak broadening reached 4 KeV (FWHM) at 200 volts. For Co 57 a resolution of 1.7 KeV (FWHM) was obtained. These values, although not exceptional, were considered satisfactory to attempt construction of a matrix.

Contact to the p side of this diode during all measurements was made with an intervening indium pad to prevent damage to the fragile structure at the gallium-indium layer. It was hoped that a reliable technique might be developed that would allow the use of this type of p type contact in an orthogonal strip matrix structure. Chordal sections cut from the diode in forming a rectangular shape were used to test both masking procedures and

---

*General Electric Research and Development Lab, Schenectady, N. Y.

Leakage current and capacitance versus reverse bias
Ultra pure p-type germanium diode 402
thickness - 4.2 mm, area 2.3 cm^2
impurity concentration - 3 - 5.6 x $10^{10}/cm^3$

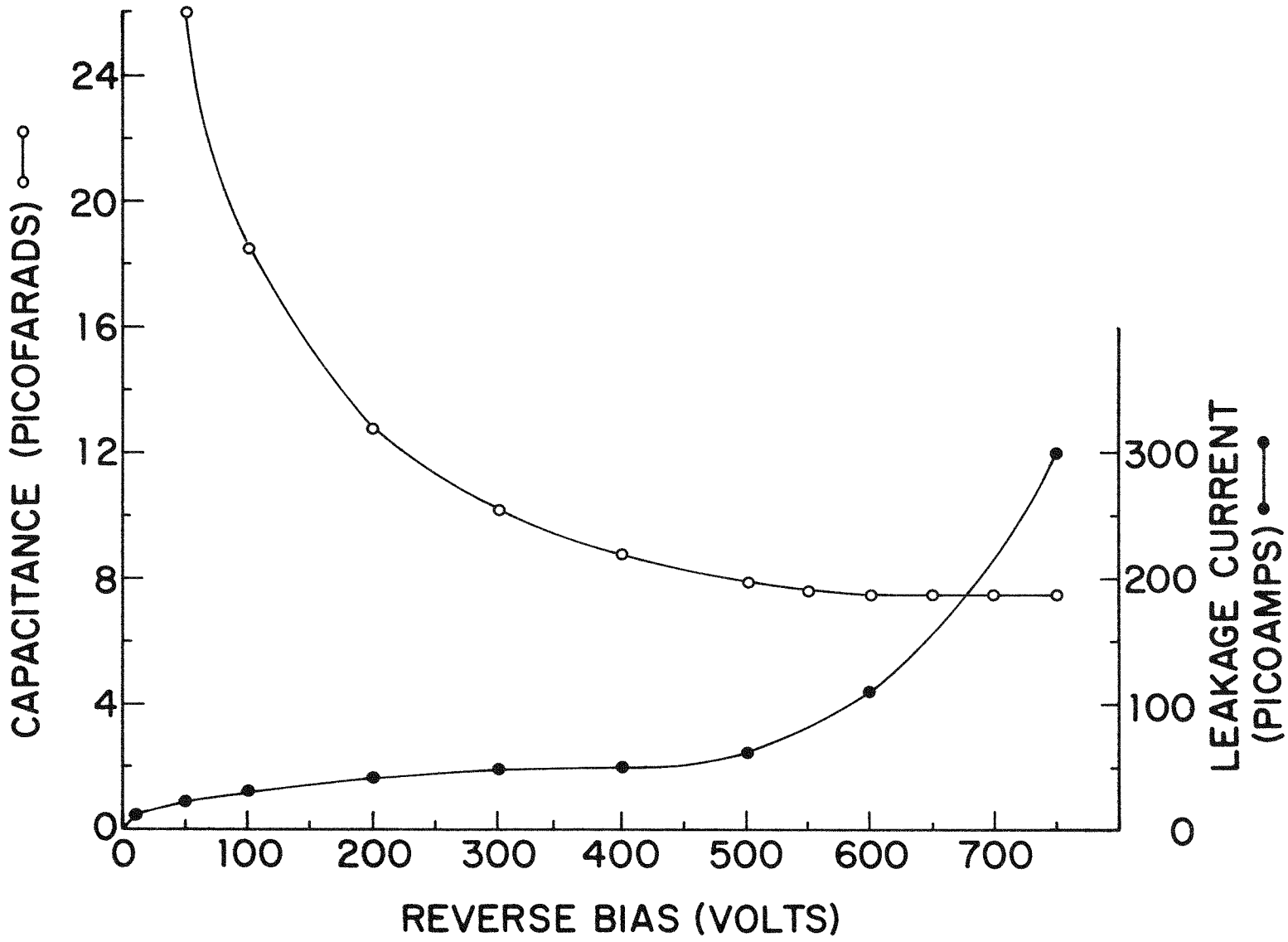

Fig. XVI

contacts with respect to potential damage that might be inflected on the p-side contact in the handling and operation of a matrix. The worst mechanical problem in using this type of p contact on a matrix was the making of non-damaging contact. An attempt to use electroless plating to construct a protective layer over this surface failed to reduce its susceptability to damage by the type pressure contacts required for an orthogonal strip matrix. Finally, it was decided that the use of this type of p^+ contact was not feasible.

Two additional circular pieces of p-type ultra-pure germanium from crystal number 413 were purchased from the same vendor. These wafers were 4 and 5 mm in thickness upon receipt and almost 3 cm in maximum diameter. The p^+ contact (Boron) for both pieces was applied by R.N. Hall at General Electric using a BF_3 glow discharge. Construction of the n^+ layer and further processing were completed at Sloan Kettering. Although the boronated p^+ layer is estimated to have a thickness of only a couple of hundred Angstroms (30) and is quite susceptible to scratch damage, the character of this p^+ surface seemed more amenable to protection than the corresponding gallium-indium contact with its delicate micro-crystallites or the alternative gold surface barrier. This indeed proved to be the case.

After the construction of the n^+ lithium diffused contact was complete, on the 5 mm thick diode it was cut into a nearly square rectangle (2.04 x 1.92) cm. After lapping and chemical processing, using standard techniques, testing was begun.

Leakage current versus reverse bias and capacitance versus reverse bias measurements for the diode are shown in figure XVII. The initial results were poor since breakdown occurred above 150 volts. The theoretical depletion voltage appropriate to the diode's thickness (4.8 mm) and specified impurity concentration is around 200 volts. The capacitance versus voltage curve taken at this time flattened near this value of bias voltage but the inferred impurity concentration ranged from about $1.5 \times 10^{10}/cm^3$ to $1.8 \times 10^{10}/cm^3$, compared to the specified $1.6 \times 10^{10}/cm^3$ of the supplier.

Subsequent reprocessing led to the next set of I-V, C-V data of figure XVIII. The breakdown voltage rose to over 280 volts. The impurity concentration obtained from the capacitance voltage curve was $1.6 \times 10^{10}/cm^3$ or less for biases under 160 volts.

Spectral data for the diode were taken for Co 60 (1172, 1333 KeV) and Co 57 (122 KeV 80%) and are shown in figures XIX and XX. These data were considered a satisfactory basis to attempt formation of an orthogonal strip matrix.

2. Orthogonal Strip Matrix Fabrication

The diode was mounted on a carbon block and grooves were cut in the p and n side with a diamond wheel attached to a surface

Leakage current and capacitance versus reverse bias
Ultra pure germanium diode 413-1 (after first etch)
thickness - 4.8 mm, area 4 cm^2
impurity concentration - $1.6 \times 10^{10}/cm^3$

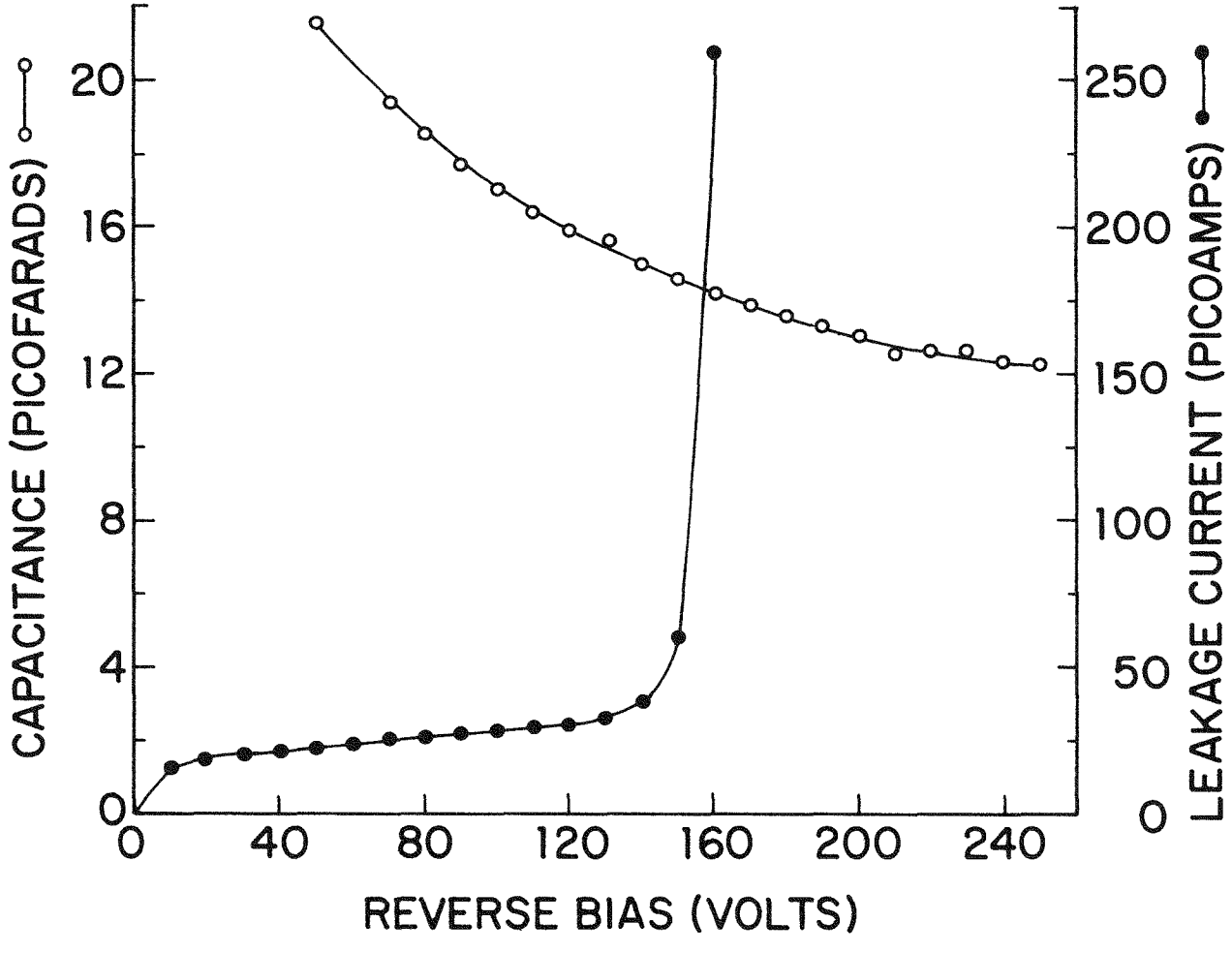

Fig. XVII

Leakage current and capacitance versus reverse bias
Ultra pure germanium diode 413-1 (after second etch)

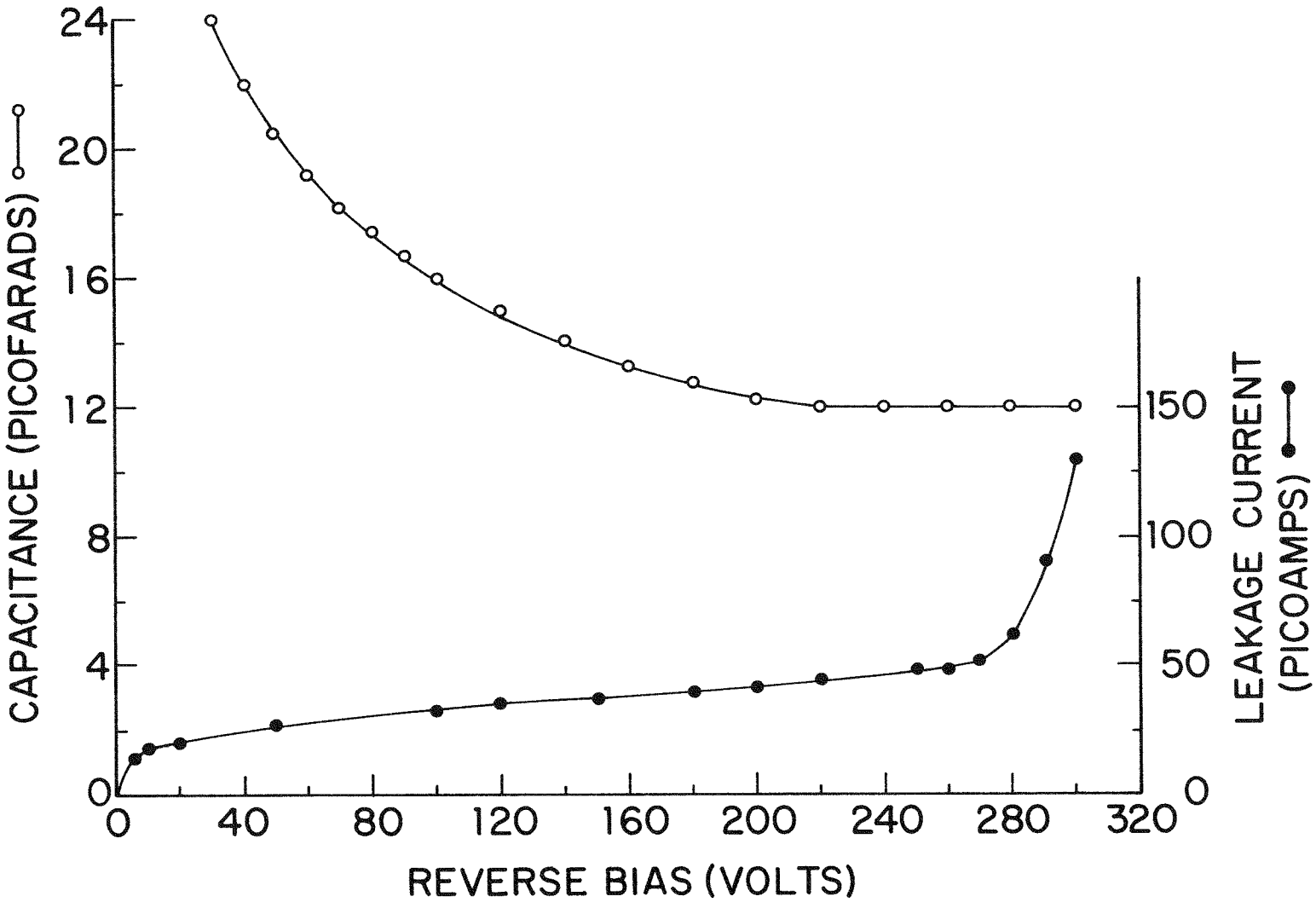

Fig. XVIII

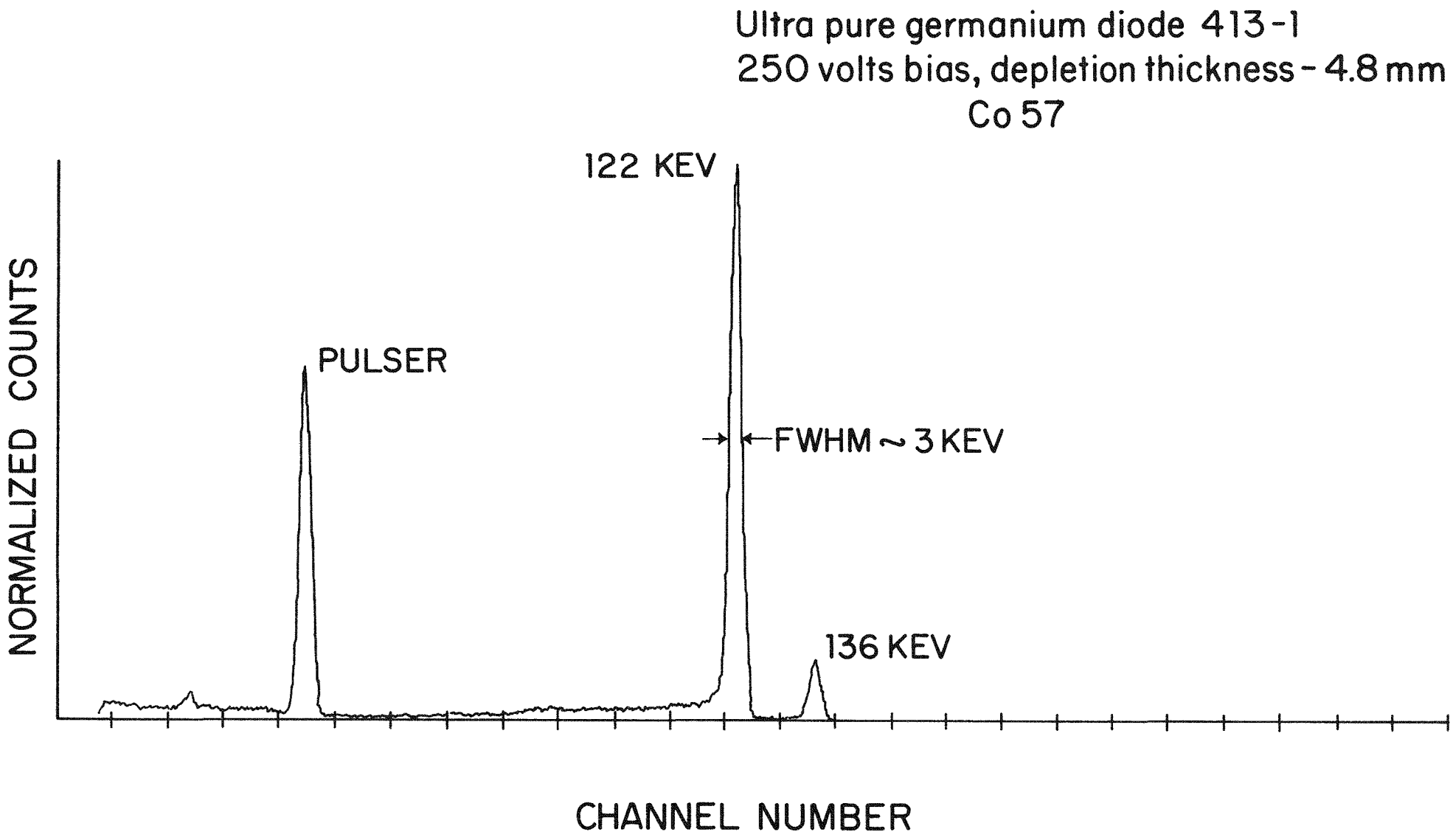
Ultra pure germanium diode 413-1
250 volts bias, depletion thickness - 4.8 mm
Co 57
122 KEV
PULSER
FWHM ~ 3 KEV
136 KEV
NORMALIZED COUNTS
CHANNEL NUMBER

Fig. XIX

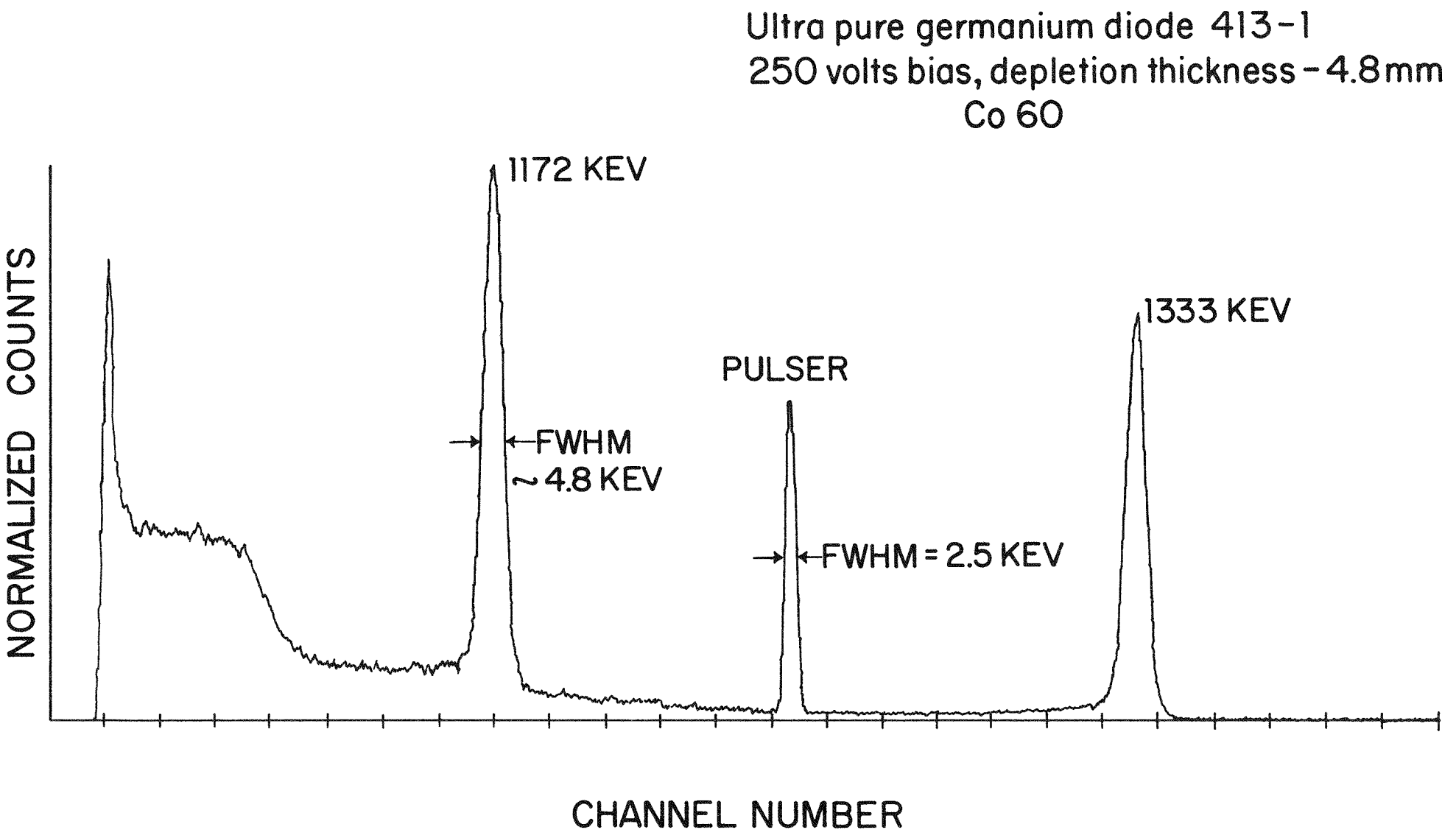
Ultra pure germanium diode 413-1
250 volts bias, depletion thickness - 4.8mm
Co 60
1172 KEV
1333 KEV
PULSER
FWHM
~ 4.8 KEV
FWHM = 2.5 KEV
NORMALIZED COUNTS
CHANNEL NUMBER

Fig. XX

grinder. The groove width used at present is .020 inch. The groove depth on the p side is ½ mm, on the n side 1 mm deep. Since the original wafer of germanium used to construct the diode was not circular, the planar dimensions of the diode cut from the piece are not square. Therefore the electrode strip widths are slightly different from the p to the n side, being 2.9 mm wide on the p side and 2.7 mm wide on the n side. Microscopic inspection after cutting of the grooves confirmed that no damage had occurred as in the prior lithium drifted unit which had reached this stage.

Following cutting of the grooves, the matrix was suitably masked and etched to remove the saw damage. Upon completion of the surface preparation, the matrix was inserted into its special cryostat and testing was begun.

3. Experimental Apparatus

The pulse measuring electronics employed at present to evaluate the initial ultra-pure germanium matrix include a group of twelve PASCA 817's manufactured by Canberra Industries. These units were built by the vendor to serve the experimental work at Sloan Kettering with the gamma camera. The designation PASCA is for preamplifier-amplifier-single channel analyzer. The circuitry for these three functions is enclosed in a double width nuclear instrumentation module.

The experimental apparatus which is employed to test and operate the germanium matrix as a "camera" is shown in figure XXI. Part of this equipment represents a modification of the apparatus which was discussed in the previous report (5) and which was based on an adaptation of a conventional cryostat. A larger diode chamber was constructed to provide adequate space.

The lower section of the prototype camera housing is the dual chamber vacuum cryostat which was also reported previously and which permits the cryostat pumping system to be self contained and compact without dependence on external power after working vacuum is established. An infra-red shield was incorporated into the matrix cryostat to lower the temperature at the matrix platform. Thermocouple measurements indicate an operating temperature of 105^{o}K.

4. Preliminary Results from Germanium Camera

Preliminary data taken for this first ultra-pure germanium orthogonal strip matrix are very encouraging. Figures XXII, XXIII show representative data for response of a cell of the matrix to a 1 mm diameter Co 57 beam probe. The source is inside the matrix cryostat above the matrix and can be positioned thorugh the operation of a rotary and translational feed-through consisting of a 1/4 inch rod which is mounted in a glass vacuum window at the top of the cryostat.

In these measurements the source is positioned above the

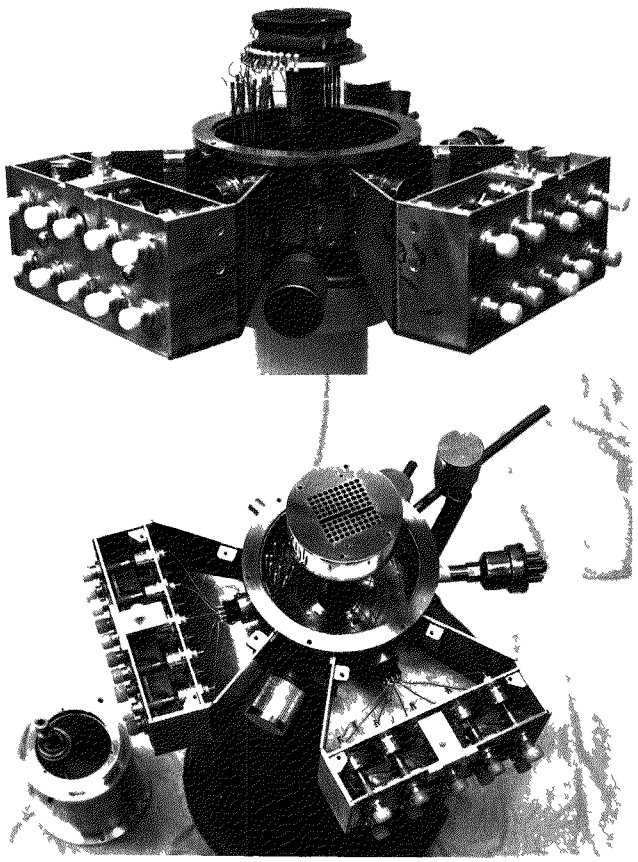

Fig. XXI Experimental apparatus used to test and operate prototype ultra-pure germanium gamma camera

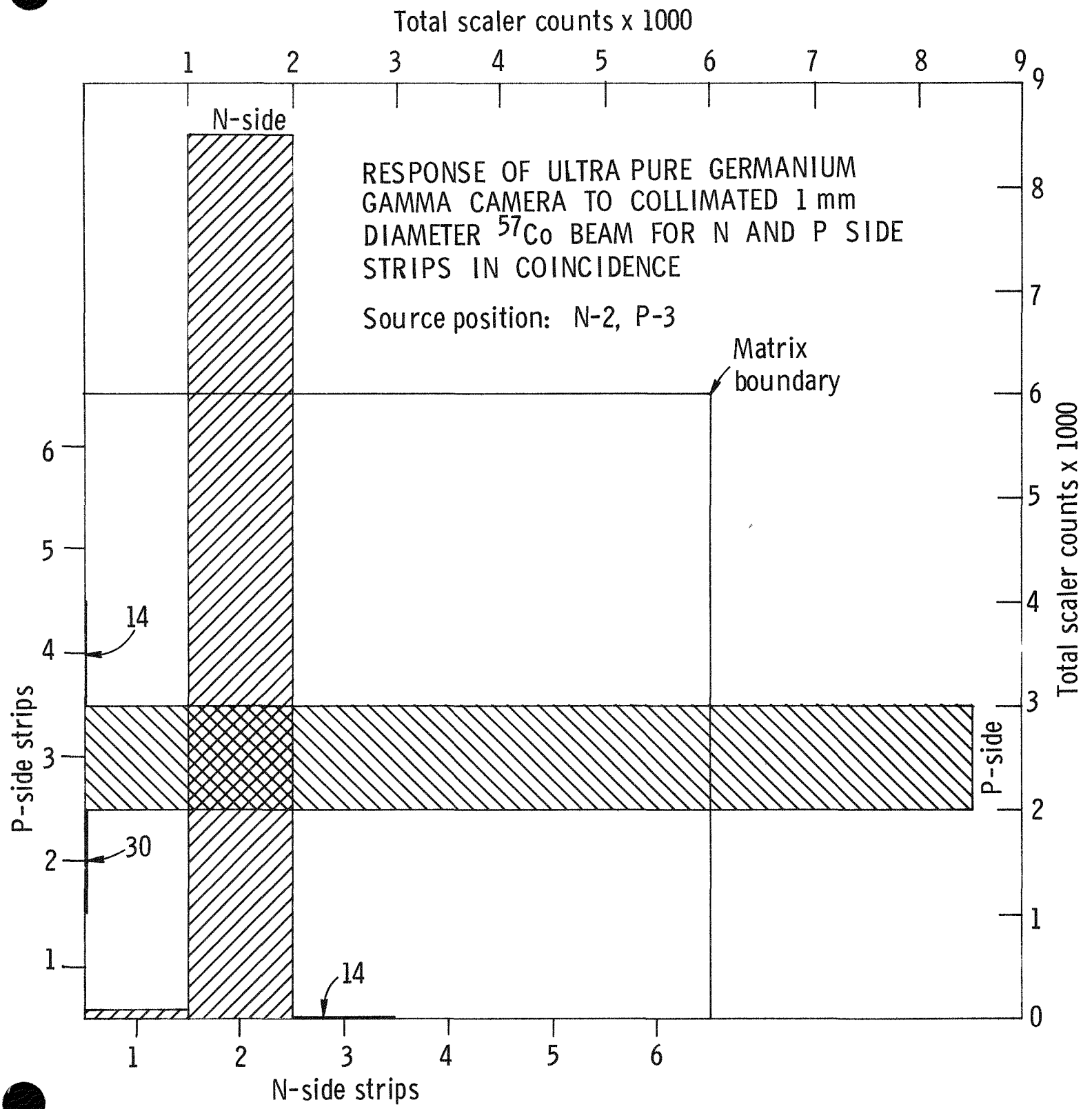
Total scaler counts x 1000
1 2 3 4 5 6 7 8 9
N-side
RESPONSE OF ULTRA PURE GERMANIUM GAMMA CAMERA TO COLLIMATED 1 mm DIAMETER ^{57}Co BEAM FOR N AND P SIDE STRIPS IN COINCIDENCE
Source position: N-2, P-3
Matrix boundary
14
30
14
P-side
P-side strips
N-side strips
Total scaler counts x 1000

Fig. XXII

CROSS TALK MEASUREMENTS WITH N AND P-SIDE STRIPS IN COINCIDENCE

Position of 1 mm ^{57}Co beam is N-2, P-3

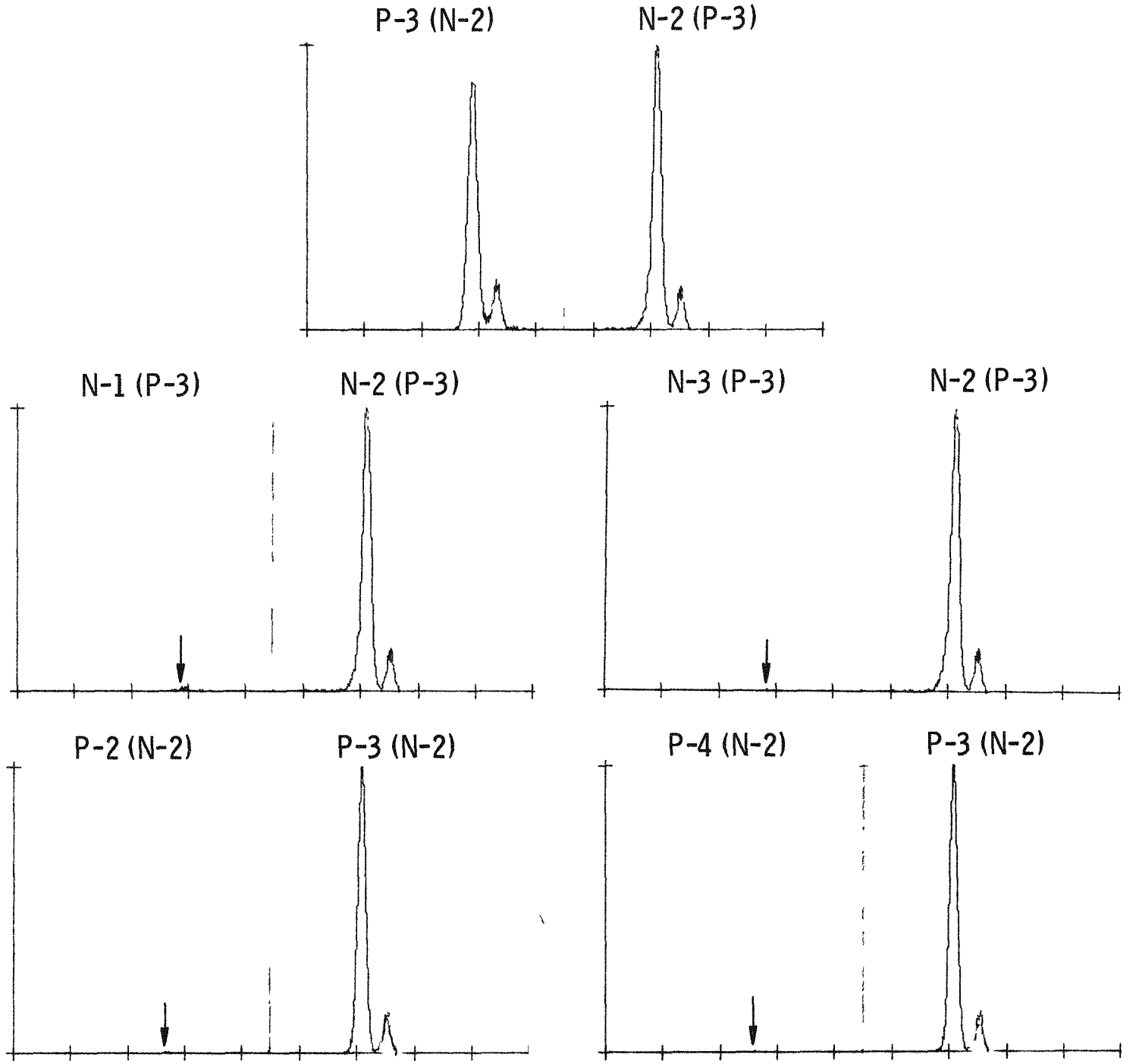

Fig XXIII

intersection of strips n-2 and p-3. The n and p side strips are monitored in coincidence. The method by which these signals are used to obtain incident gamma-ray position information is shown schematically in figure XXIV. The collimator indicated in this figure is replaced by the collimated 1 mm beam Co 57 source. For these measurements the single channel analyzer window was set wide enough to admit both the 122 KeV (80%) and 136 KeV peaks. In actual operation the 136 KeV peak would be excluded by narrowing the window setting.

Referring back to figure XXIV, the total scaler count for both p and n sides is shown at the top and bottom of the page. The six n and p side electrode strips are indicated, as is the matrix boundary. The corresponding spectral measurements for the same source position are shown in figure XXIII. It can be seen that an insignificant number of pulses pass through the SCA window in the strips adjacent to those which intersect beneath the source. Thus an operational resolution of within (3.5 x 3.5) mm is demonstrated. The corresponding computer generated isometric image of this 1 mm beam source is shown in figure XXV.

The effective quantum efficiency of this camera is still to be measured. This will be done with a calibrated, collimated Co 57 beam probe. Major interest exists in Tc^{99m} (140 KeV) because of the clinical significance of this isotope. An estimate based on first collision yields a figure of well over 20 per cent for photoelectric efficiency for the thickness of the prototype germanium matrix.

Multichannel analyzer measurements of the spectral response of each matrix cell to an uncollimated, 1 millicurie Co 57 source outside the cryostat indicates that all cells are operative with resolution more than adequate for gamma camera operation. This was inferred from the multichannel analyzer display as a preliminary inspection. More quantitative measurements will be made within the present contract period.

Measured spectral response to Co 57 is shown in figures XXVI and XXVII for an n and p side strip measured in coincidence. No single channel analyzer was used to exclude low energy pulses. The low energy secondary peaks have been verified as being within a few microsecond coincidence window and may be due to charge loss at the boundary of the strips. Further measurements are needed to determine this.

Additional measurements are in progress. Some of these include the determination of the effective "dead width" of the grooves between electrode strips on both n and p sides of the germanium matrix and the groove resistance values on each side of the device. The latter values are expected to correlate to the "cross-talk" between electrode strips particularly with respect to charge loss at the boundaries of the electrode strips. Such losses to neighboring strips will adversely affect spatial resolution. Variations in such characteristics with reverse bias will also be determined.

POSITION INDICATION FOR GAMMA RAY ABSORBED IN ORTHOGONAL STRIP MATRIX

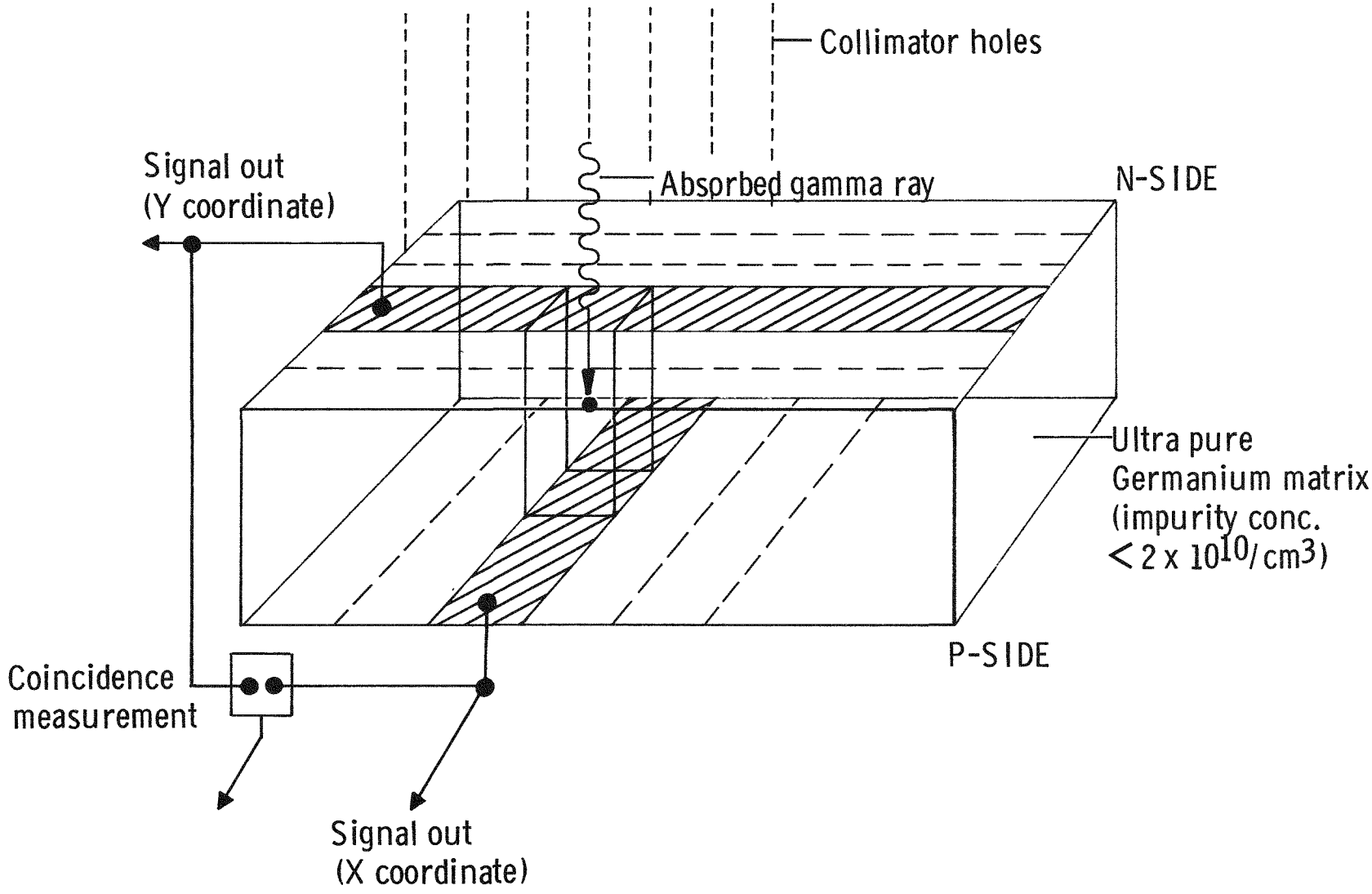

Fig. XXIV

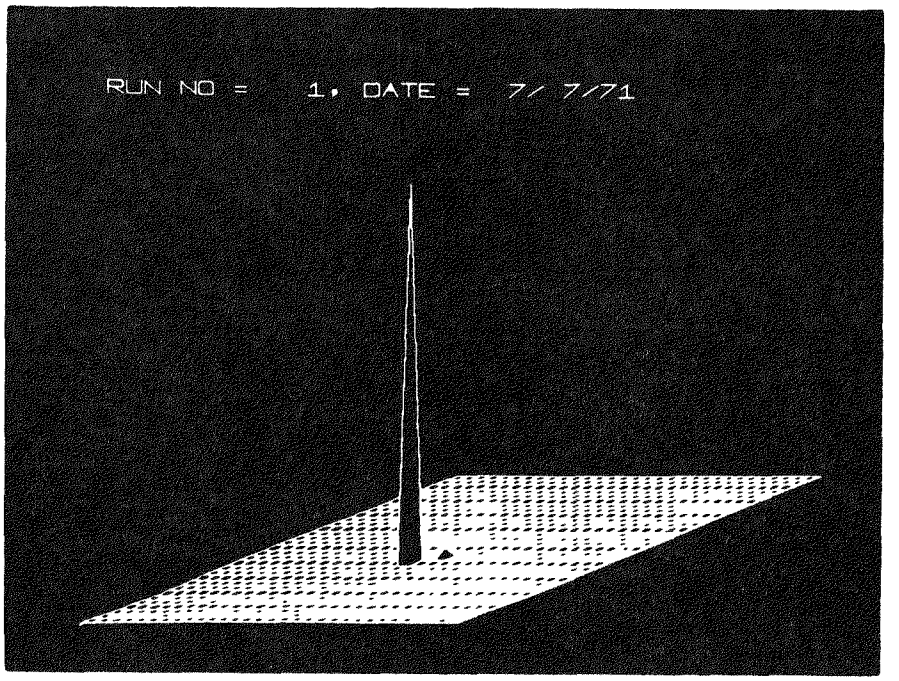

Fig. XXV Computer generated image of 1 mm diameter Co 57 beam from ultra-pure germanium gamma camera

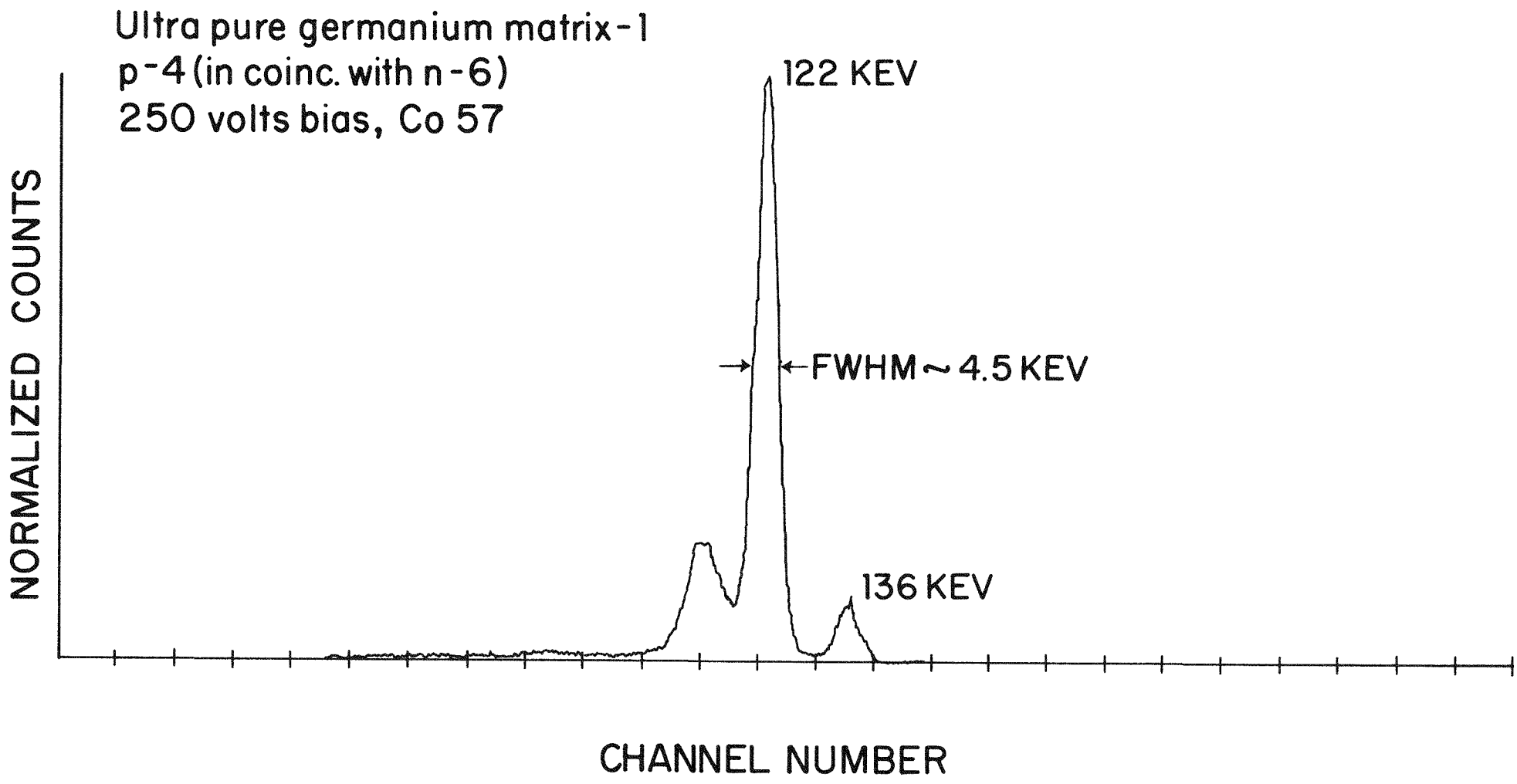
Ultra pure germanium matrix-1
p-4 (in coinc. with n-6)
250 volts bias, Co 57
122 KEV
FWHM ~ 4.5 KEV
136 KEV
NORMALIZED COUNTS
CHANNEL NUMBER

Fig. XXVI

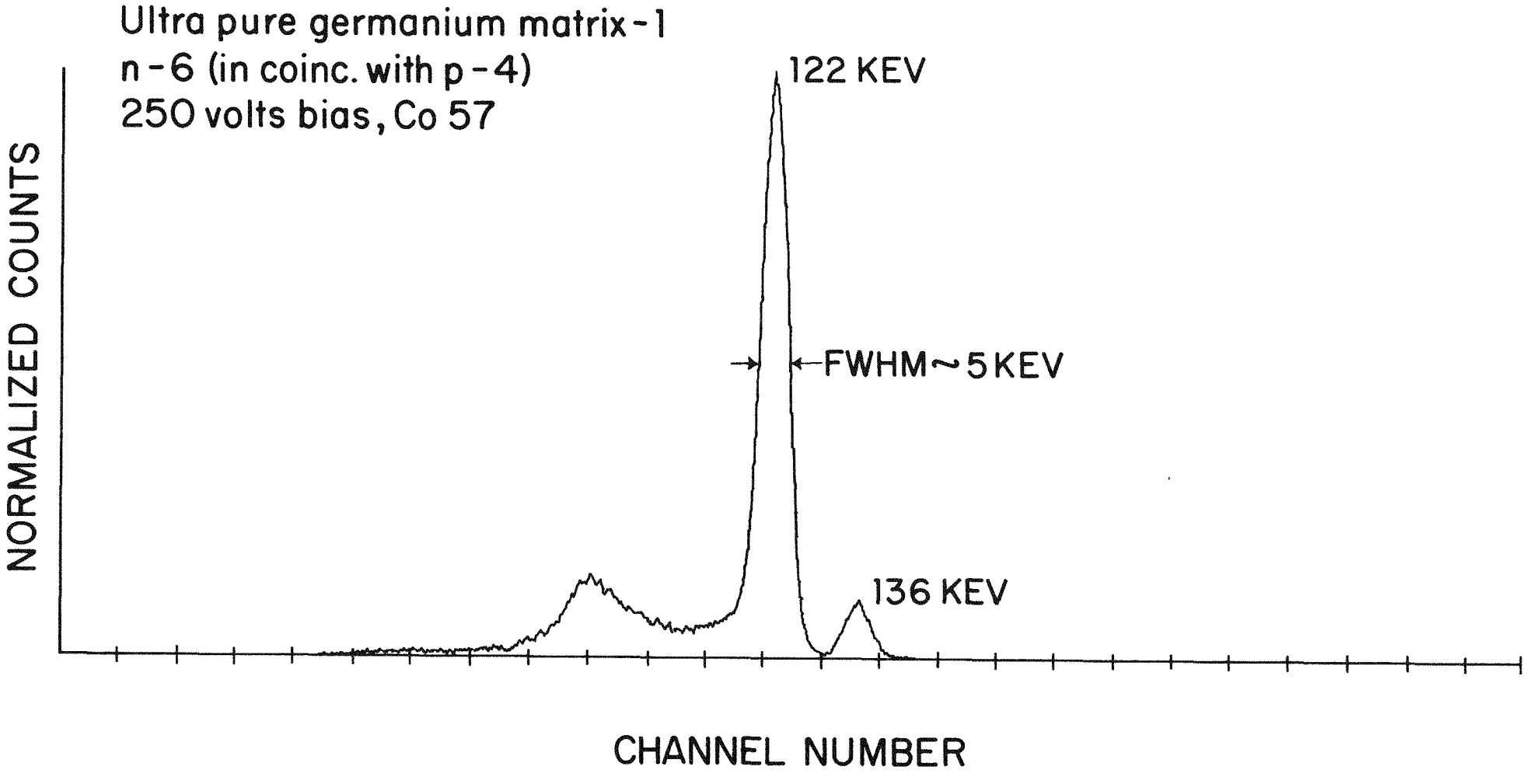
Ultra pure germanium matrix-1
n-6 (in coinc. with p-4)
250 volts bias, Co 57
122 KEV
FWHM ~ 5 KEV
136 KEV
NORMALIZED COUNTS
CHANNEL NUMBER

Fig. XXVII

Some variation in resistivity and pulse height across the germanium wafer is possible. The extent of these effects on the charge collection characteristics of each matrix block is considered of major importance with respect to the construction of a larger semiconductor gamma camera. The evaluation of such effects will also be included in the future measurements program.

V. REFERENCES

1. Genna, S., and Laughlin, J.S., Local Absorbed Dose Determination by Direct Calorimetric Measurement. Radiation Res., 5:604, 1956.

2. Milvy, P., Genna, S., Barr, N. and Laughlin, J.S., Calorimetric Determination of Local Absorbed Dose. Proc. 2nd International Conference Peaceful Uses of Atomic Energy, Geneva, Vol. 21:142, Columbia Univ. Press, N.Y., 1958.

3. Geisselsoder, J., Kopke, K., and Laughlin, J.S., Calorimetric Determination of Absorbed Dose and G_{Fe}^{+++} of the Fricke Dosimeter with 10 MeV and 20 MeV Electrons, Rad. Res., 20:423, 1963.

4. Pinkerton, A.P., Comparison of Calorimetric and other Methods for the Determination of Absorbed Dose. Annal. N.Y. Acad. of Sci. 161:63, 1969.

5. Annual Progress Report to the United States Atomic Energy Commission. Contract AT(30-1)3510 Biological and Clinical Dosimetry, 1970.

6. Laughlin, J.S., and Genna, S. Calorimetry in Vol. II, Radiation Dosimetry, 389-441, Edited by Attix, F.H., Roesch, W.C. and Tochlin, E. Academic Press, New York, N.Y. 1966.

7. McLaughlin, W.L., Hussmann, E.K., Eisenlohr, H.H. and Chalkley, L., A Chemical Dosimeter for Monitoring Gamma Radiation Doses of 1-100 kilorads. Int. J. Appl. Rad. & Isotopes, 22:135, 1971.

8. McLaughlin, W.L., Microscopic Visualization of Dose Distributions. Int. J. Appl. Rad. & Isotopes, 17:85, 1966.

9. McLaughlin, W.L., Radiochronic Dye-Cyanide Dosimeters in Manual on Radiation Dosimetry, pp.377-395, Edited by Holm Niels, W., and Berry Roose, J. Martel Deteker, Inc., N.Y. 1970.

10. Rossi, H.H., Microscopic Energy Distribution in Irradiated Matter, in Vol.I. Radiation Dosimetry, 43-90, Edited by Attix, F.H., Roesch, W.C. and Tochlin, E., Academic Press, New York, N.Y. 1968.

11. Lucas, A.C. Characteristics of a 2 inch Spherical Proportional Counter Tech. Note S-70-TN, Oct., 1968, E.G.& G. Inc., Goleta, Calif.

12. Evans, R.G., Pinkerton, A.P., Djordjevic, B., Mamacos, J.P., and Laughlin, J.S. Changes in Biological Effectiveness of a Fast Neutron Beam with Depth in Tissue Equivalent Material. Radiation Research, 45:235, 1971.

13. Berry, R.J., The Role of Factors Modifying Neutron Damage in Irradiation of Mammalian Cells In Vitro and In Vivo. Proc. Symp. Neutrons in Radiobiology, p.483, Oak Ridge, Tennessee, 1969.

14. Nias, A.H.W., Changes in the Biological Parameters for Mammalian Cells as a Function of Positron in a 14 MeV Field. Presented at the IVth International Congress of Radiation Research, Evian, France, July, 1970.

15. McNally, N.J. and Bewley, D.K., A Biological Dosimeter Using Mammalian Cells in Tissue Culture and its Use in Obtaining Neutron Depth Dose Curves. Br. J. Radiology, 42:289, 1969.

16. Broerse, J.J., Effects of Energy Dissipation by Monoenergetic Neutrons in Mammalian Cells and Tissues. Radiobiological Institute TNO, Rijswijk, The Netherlands.

17. Fairchild, R.G., Sources of Fission Neutrons and Their Dosimetry. U.S. Atomic Energy Commission Report BNL-12452 (CONF.-680420-2) 1968.

18. Krishnaswamy, V. and Colvett, R.D., Personal Communication, Brookhaven National Laboratory, Upton, New York.

19. Oliver, G.D., and Wright, C.N., Dosimetry of an Implantable ^{252}Cf Source. Radiology 92:143, 1969 (As Revised).

20. Epp, E.R., Weiss, H. and Santomasso, A., The Oxygen Effect in Bacterial Cells Irradiated with High Intensity Pulsed Electrons. Radiation Research, 34:320-325, 1968.

21. Epp, E.R., Weiss, H., Santomasso, A., and Heslin, J., New Upper Limit to the Lifetime of Oxygen Sensitive Species Suspected to be Induced at Critical Sites in Irradiated Bacterial Cells. Presented at Rad. Res. Soc. Meeting, Boston, 1971.

22. American Institute of Physics Handbook, Chapt. 8, p.39.

23. Annual Progress Report, Biological and Clinical Dosimetry, AEC Contract AT(30-1)3510, 1967.

24. Bennett, W.H., Magnetically Self-Focusing Streams. Phys. Rev. 45:890, 1934.

25. McDonald, J., Weiss, H., Pinkerton, A., and Epp, E.R., Electronic Monitoring of Nanosecond Pulses from a Field Emission Electron Source. Radiat. Res. 43:514- 524, 1970.

26. Berger, M.J., Review and Updating of Information on Transmission and Reflection of Electrons by Aluminum Shields. National Bureau of Standards Memorandum, August, 1970.

27. Berger, M.J. and Seltzer, S.M., Tables of Energy Losses and Ranges of Electrons and Positions. N.A.S.A. S.P.-3012, 1964.

28. Willis, C., Boyd, A.W., and Miller, O.A., The Absolute Dosimetry of High Intensity, 600 KV Pulsed Electron Accelerator Used for Radiation Chemistry Studies of Gaseous Samples. Rad. Res. 46:428, 1971.

29. Llacer, J., Private Communication. Instrumentation Group, Brookhaven National Laboratories, Upton, N.Y.

30. Baertsch, R.D., Private Communication, General Electric Research and Development Laboratory, Schenectady, N.Y.

VI. PUBLICATIONS AND PRESENTATIONS

Publications

1. Detko, J. A Dual Chamber Vacuum Cryostat Ion Germanium Lithium Drifted Diodes. Letter to the Editor, Nuclear Instruments and Methods, 94:395, 1971.

2. Epp, E.R. Response of cells to high-intensity pulsed radiation and possibilities for measuring oxygen diffusion times in cells. Annals of the New York Academy of Sciences 32:253-261, 1970.

3. Evans, R.G., Pinkerton, A.P., Djordjevic, B., Mamacos, J., and Laughlin, J.S. Changes in Biological Effectiveness of a Fast Neutron Beam with Depth in Tissue-Equivalent Material. Radiation Research, 45:235-243, 1971.

4. McDonald, J., Weiss, H., Pinkerton, A.P. and Epp, E.R., Electronic Monitoring of Nanosecond Pulses from a Field Emission Source. Radiation Research, 43:514-524, 1970.

5. McDonald, J., Pinkerton, A., Weiss, H., and Epp, E.R. Dosimetry for Thin Biological Samples Irradiated by Nanosecond Electron Pulses. Radiation Research (in press).

6. Pinkerton, A., Mamacos, J., and Laughlin, J.S., Dosimetry of Fast Neutron Beams from a Small Medical Cyclotron. Radiology 96:131, 1970.

Presentations

1. Epp, E.R., Weiss, H., Santomasso, A. and Heslin, J.M., Response of bacterial cells to double pulses of high-intensity electrons from field emission sources. Paper presented at the 4th International Congress of Radiation Research, Evian, France, June, 1970.

2. Epp, E.R., and Weiss, H., Sensitivity of living cells to high-intensity pulses of ionizing radiation and measurements relating to oxygen diffusion times in cells. Paper presented at the Meeting of the American Physical Society, New Orleans, Louisiana, November, 1970.

3. Epp, E.R., Rapid remote controlled, high dose rate, intracavitary techniques in cancer management. Paper presented at the New York Academy of Medicine, Symposium, New York, New York, December, 1970.

4. Evans, R.G., Pinkerton, A.P., Djordjevic, B., Mamacos, J., and Laughlin, J.S., Biological Effectiveness and Oxygen Dependence of Fast Neutron Beams at Different Depths of Tissue Equivalent Materials. Presented at the Radiation Research Society Meeting, Dallas, March, 1970.

5. Holt, J.G., Pinkerton, A.P., Laughlin,J.S., and Hilaris, B.S., Dosimetric Consideration in the Interstitial Use of Encapsulated Iodine-125 Sources. Presented at Annual Meeting of the American Radium Society, Mexico City, March, 1971.

6. McDonald, J., Pinkerton, A., Weiss, H., and Epp, E.P., Dosimetry for Thin Biological Samples Irradiated at Ultra-High Dose Rates by Electron Pulses of Nanosecond Durations. Presented at the Radiation Research Society Meeting, Boston, Mass., May, 1971.